Check for updates

Recent progress in layered metal halide perovskites for solar cells, photodetectors, and field-effect transistors

Chwen-Haw Liao, Md Arafat Mahmud and Anita W. Y. Ho-Baillie [iD] *

Metal halide perovskite materials demonstrate immense potential for photovoltaic and electronic applications. In particular, two-dimensional (2D) layered metal halide perovskites have advantages over their 3D counterparts in optoelectronic applications due to their outstanding stability, structural flexibility with a tunable bandgap, and electronic confinement effect. This review article first analyzes the crystallography of different 2D perovskite phases [the Ruddlesden–Popper (RP) phase, the Dion–Jacobson (DJ) phase, and the alternating cations in the interlayer space (ACI) phase] at the molecular level and compares their common electronic properties, such as out-of-plane conductivity, crucial to vertical devices. This paper then critically reviews the recent development of optoelectronic devices, namely solar cells, photodetectors and field effect transistors, based on layered 2D perovskite materials and points out their limitations and potential compared to their 3D counterparts. It also identifies the important application-specific future research directions for different optoelectronic devices providing a comprehensive view guiding new research directions in this field.

1. Introduction

Metal halide perovskites are highly versatile semiconducting materials due to their long charge carrier lifetime, high light absorption coefficient, and narrow emission bandwidth.[1–7] They have attracted significant research attention worldwide in materials science, physics, and chemistry. In 2009, Kojima *et al.* first demonstrated a solar cell using a metal halide perovskite as an active layer producing a power conversion efficiency (PCE) of ~3.8%.[8] Incredible performance improvement in halide perovskite solar cells has since been achieved reaching a certified PCE of 25.7% in 2022.[9] Moreover, metal halide perovskites have immense potential for various optoelectronic devices, such as light-emitting diodes, field-effect transistors, and photodetectors, due to their excellent optical and electronic properties.[10–14] Three-dimensional (3D) perovskites have been extensively studied with an empirical formula of ABX_3 (Fig. 1) and a crystal structure with the corner-sharing six-coordinated octahedra, where A is monovalent cations (Cs^+, Rb^+, $MA^+ = (CH_3NH_3)^+$, or $FA^+ = (CH(NH_2)_2)^+$), B is divalent metal cations (Pb^{2+} or Sn^{2+}), and X is halide anions (Cl^-, Br^-, or I^-). The probable crystallography can be deduced by the Goldschmidt factor (t) on whether a 3D or 2D perovskite structure is formed.[6,15] t is defined as the ratio of the distance

between A–X and B–X according to the idealized solid-sphere model ($t = (R_A + R_X / \sqrt{2}(R_B + R_X))$), where R_A, R_B, and R_X are the corresponding effective ionic radii. Typically, a 3D perovskite has a Goldschmidt factor in the range of 0.81 to 1.11, whereas a 2D perovskite would have a value higher than 1.11. The ABX_3
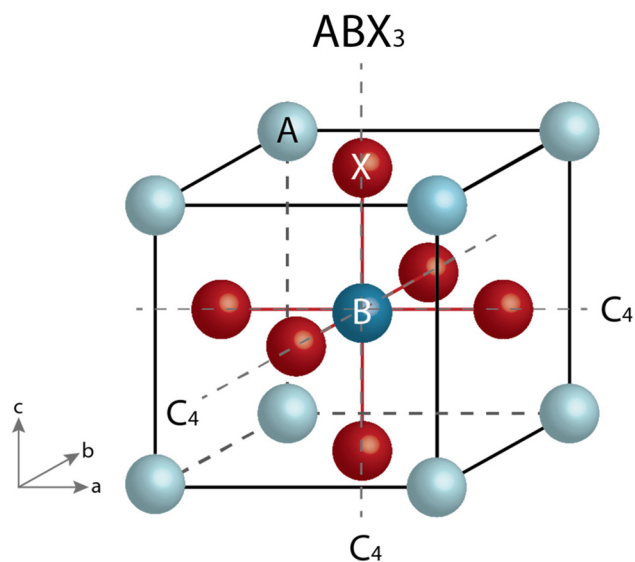

Fig. 1 The perovskite crystal structure with the molecular formula of ABX_3 (A: Cs^+, Rb^+, $MA^+ = (CH_3NH_3)^+$, or $FA^+ = (CH(NH_2)_2)^+$; B: Pb^{2+} or Sn^{2+}; and X: Cl^-, Br^-, or I^-).

School of Physics, University of Sydney Nano Institute, The University of Sydney, Sydney, NSW, 2006, Australia. E-mail: anita.ho-baillie@sydney.edu.au

3D structure can contain a small organic cation at the A site. A large organic cation with a long carbon chain cannot be integrated into a 3D structure that forms a two-dimensional (2D) structure. The 2D perovskite can be imaged by slicing the 3D structure along the crystallographic plane, forming sheets, and inserting the halide anions at the $[BX_6]^{2-}$ octahedra corner to satisfy the centre metal coordination and then adding the large cation as a spacer between the inorganic sheets. The cleaving can be done along three different planes of the 3D structure to establish the ⟨100⟩, ⟨110⟩, and ⟨111⟩ oriented 2D perovskites. Notably, this molecular-level dimension reduction differs at the morphology level, in which the framework remains the same but the crystallite size changes. At the morphology level, the system shows size-dependent properties at the nanoscale. For instance, as the morphology changes, $MAPbI_3$ results in a 3D nanocube, a 2D nanoplate, and a 1D nanowire. Importantly, all of them are 3D materials in solid-state definition with the molecular formula of ABX_3 and limited candidates due to the same framework. Therefore, molecular-level 2D metal halide perovskites demonstrate various kinds of spacers and come with a tunable bandgap, unique structure confinement properties, and long stability. This review will focus on molecular-level 2D metal halide perovskites with different crystallographic phases for different types of semiconducting applications.

2. Low-dimensional layered metal halide perovskites

More than 700 types of 2D metal (Pb or Sn) halide perovskites have been reported to date, demonstrating a remarkable structural diversity and tunable optoelectronic properties by different thicknesses, cage cations, and spacer cations.[16,17] They can be classified into three categories: the Ruddlesden–Popper (RP)[18] phase, the Dion–Jacobson (DJ)[19] phase, and the alternating cations in the interlayer space (ACI)[20] phase as shown in Fig. 2 with the general formulae of $A_2A'_{n-1}B_nX_{3n+1}$, $AA'_{n-1}B_nX_{3n+1}$, and $AA'_nB_nX_{3n+1}$, respectively.

2.1 Ruddlesden–Popper (RP) phase perovskites

The most common layered metal halide perovskites are based on the RP structure with long monoammonium chains. The general formula is $A_2A'_{n-1}B_nX_{3n+1}$, in which the A cation is the long carbon chain spacer and the A′ cation is the small cation (MA^+, FA^+, or Cs^+). They usually interdigitate between the $[BX_6]^{2-}$ inorganic stack and present a large separation, also known as d spacing (indicated in Fig. 2) albeit insulating. The inorganic layers in the RP phase structure are offset by one octahedral unit with (1/2, 1/2) displacement through the ab-plane. Therefore, inorganic layers slide in a staggered composition in which the $[BX_6]^{2-}$ octahedral unit is not perfectly stacked on top of one another. Due to this, the spatial confinements of the charge carrier and the dielectric contrast between the inorganic stack and the organic spacer increase resulting in a high exciton binding energy around 150 to 500 meV, typically ten times larger than those of 3D perovskites (10–50 meV).[22]

In 1994, Mitzi et al. reported the first homologous series of linear carbon chain cation 2D perovskites $(C_4N_9NH_3)_2(MA)_{n-1}Sn_nI_{3n+1}$ (n = 1–5) and their intrinsic electronic properties.[23] The Hall carrier concentration was estimated to be 7×10^{18} cm^{-3} with a low resistivity of $\sim 10^{-2}$ Ω cm for the n = 5 compound. These values set up 2D metal halide
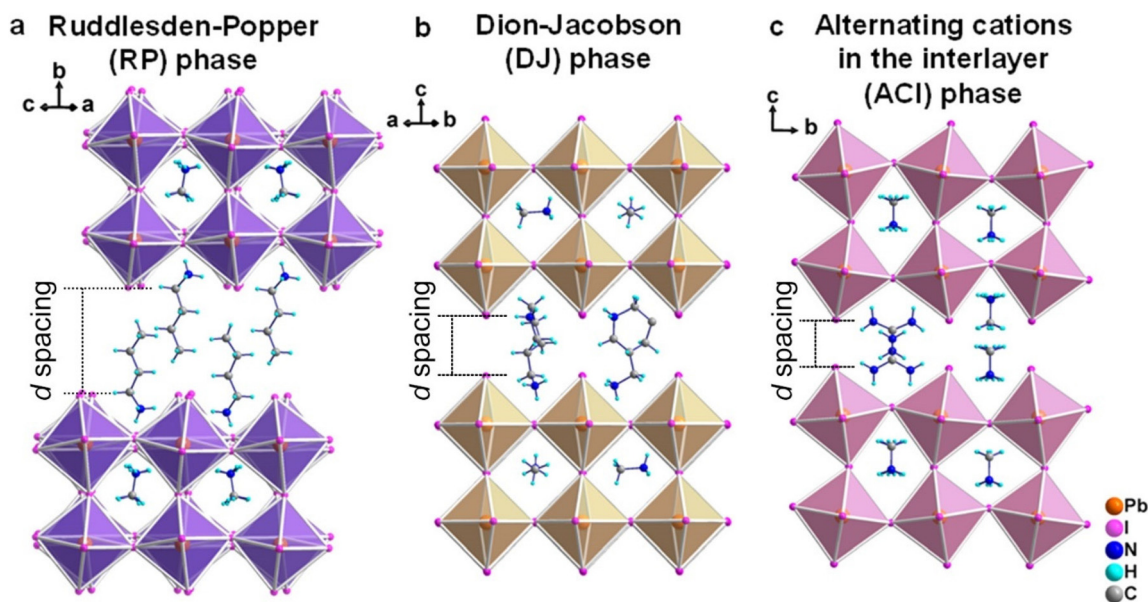

Fig. 2 Lower dimensional layered perovskite structures. (a) The Ruddlesden–Popper (RP) phase, (b) the Dion–Jacobson (DJ) phase, and (c) the alternating cations in the interlayer space (ACI) phase.[21]

perovskites as promising superconducting materials. In addition, when the layers (*n* value) of inorganic slabs increase in the 2D perovskite unit cell structure, the electronic properties become more similar to 3D perovskites but with the added advantage of 2D perovskites' higher stability and structural confinement properties. It is important to highlight that layered perovskites with *n* > 5 are synthetically challenging to be isolated into a pure phase due to the undesirable enthalpies of formation (ΔH_f). The higher *n* value component easily transfers into *n* = 3 and *n* = ∞ members.[24] In 2020, Tarasov *et al.* built a database with more than 600 kinds of RP phase layered metal halide perovskite single crystals.[17] However, none of them exceeded *n* = 5 until Soe *et al.* reported the first structural characterization of an *n* = 7 RP phase perovskite single crystal, $BA_2MA_6Pb_7I_{22}$, by kinetic control.[25] The enthalpy changes of quasi-2D perovskite formation were thoroughly investigated in this work.[25] The increase in ΔH_f with the *n* value is also observed in FA-based RP phase perovskites, similar to the case of MA-based layered perovskites.[26]

Throughout the years, RP phase perovskites have been successfully applied for solar cells,[27] light-emitting diodes,[28] photodetectors,[29] and field-effect transistors.[30] However, most of these perovskites are based on A-site-substituted layered perovskites, which have low vertical conductivity. In contrast, X-site engineering can divide the metal halide octahedron into a $[B(X_1)_4(X_2)_2]^{2-}$ framework without its corner-sharing property due to another X_2 anion occupying the axial atomic coordination position. Thus, it would lead to a minor separation between the octahedra layers increasing vertical conductivity.

To explore the potential candidates for X-site substituted perovskites, Walker and colleagues used density functional theory (DFT) to model structures with various polyatomic X-site anions that have an acceptable Goldschmidt factor, as shown in Fig. 3a.[31] While the results indicate that opportunities exist, only a few pure 2D X-site-substituted layered perovskite single crystals have been reported. In 2015, Daub *et al.* reported the first pseudohalide 2D hybrid perovskite $MA_2Pb(SCN)_2I_2$ single crystal as shown in Fig. 3b [32] and they verified that the pseudohalide SCN anion occupies the axial atomic coordinates in the octahedron. In 2018, Li *et al.* reported the first all-inorganic 2D perovskite $Cs_2PbCl_2I_2$ single crystal (Fig. 3c).[33] The I anions occupy the axial atomic position, while the Cl anions occupy the octahedron plane. In 2022, Liao *et al.* demonstrated a 2D inorganic pseudohalide perovskite $Cs_2Pb(SCN)_2Br_2$ single crystal.[34] This was the first demonstration of a 2D X-site-substituted layered perovskite with reversible phase transformation from (2D) $Cs_2Pb(SCN)_2Br_2$ to (3D) $CsPbBr_3$ at a temperature of 450 K (Fig. 3d). Due to the
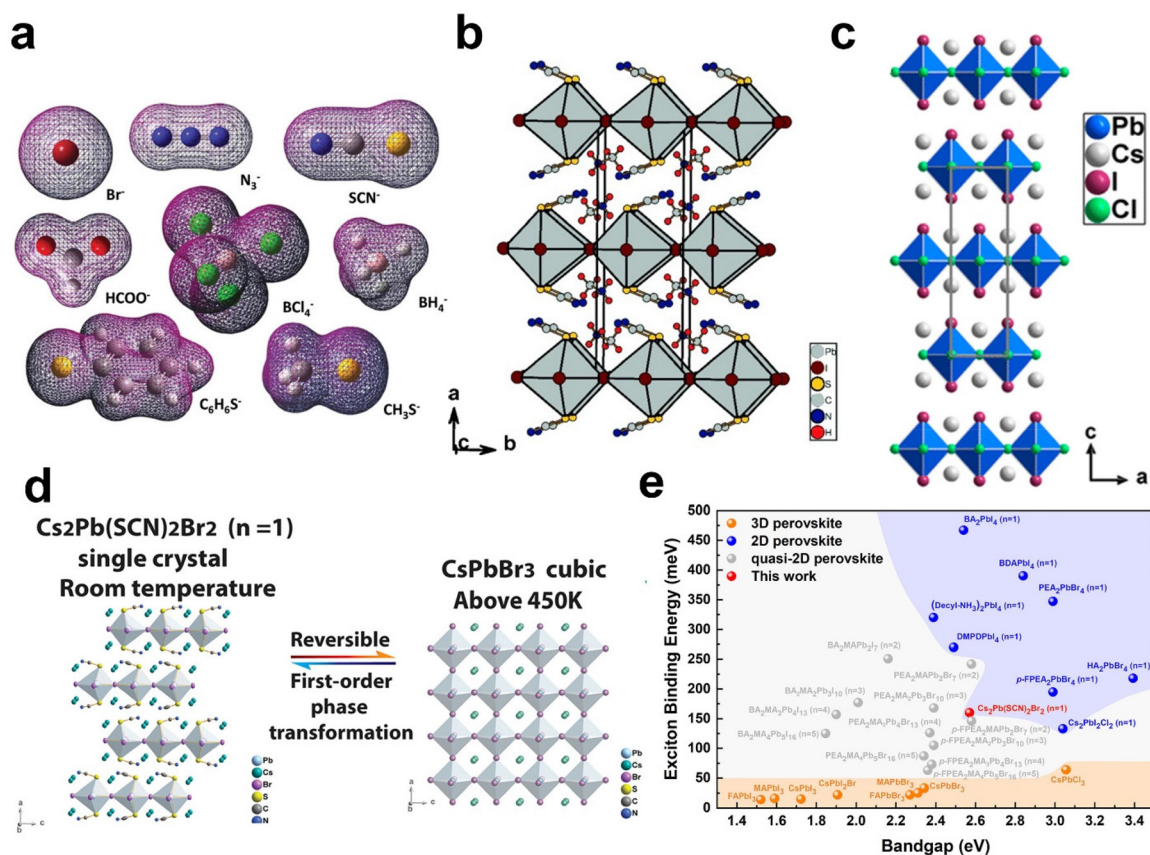
Fig. 3 Illustrations of some Dion–Jacobson (DJ) phase perovskites reported. (a) Potential X-site anions in layered perovskites investigated by DFT calculation.[31] The crystal structures of (b) $MA_2Pb(SCN)_2I_2$,[32] and (c) $Cs_2PbCl_2I_2$,[33] and (d) $Cs_2Pb(SCN)_2Br_2$ and the reversible phase transformation to the $CsPbBr_3$ phase.[34] (e) Exciton binding energy chart of some of the 2D, quasi-2D, and 3D lead halide perovskites.[34]

small separation between the $[Pb(SCN)_2Br_2]^{2-}$ inorganic slab, the single crystal demonstrates a relatively low exciton binding energy (160 meV) compared to other A-site substituted layered perovskites (>200 meV), as shown in Fig. 3e.

2.2 Dion–Jacobson (DJ) phase perovskites

DJ phase perovskites typically incorporate diammonium organic cations as a spacer—different from RP phase perovskites. The molecular formula is $AA'_{n-1}B_nX_{3n+1}$ (A cation: diammonium organic cation, A' cation: MA^+, FA^+, or Cs^+). Intriguingly, the diammonium cation can form electrostatic interaction at two separate sites (Fig. 2b), resulting in narrow separation, thus significantly limiting the transport energy barrier. In DJ phase oxide perovskites, for example, a large cation spacer corresponds to (0, 0) no shift ($P4/mmm$ space group) through the ab-plane in a unit cell, and a small cation spacer relates to the (1/2, 0) shift ($I4/mmm$ space group).[20] However, a layered hybrid halide perovskite should have more than one cation site in the interlayer per formula unit. Therefore, the DJ phase may be more appropriately referred to as a "perovskite-like" phase.[35] In 2018, Mao *et al.* reported the first homologous 3-aminomethylpiperidinium (3AMP) and 4-aminomethylpiperidinium (4AMP) series of DJ phase perovskites from $n = 1$ to 4 with the general molecular formula of $AA'_{n-1}B_nX_{3n+1}$.[19] In 2019, the same group successfully synthesized a thick $(4AMP)MA_6Pb_7I_{22}$ single crystal with seven layers (Fig. 4a).[36] They discovered that the DJ phase perovskite

has less lattice strain which causes a broader electronic band and lower bandgap energy than RP phase perovskites. In terms of thermodynamic stability, which has an implication on its extrinsic stability, some argued that the DJ phase is less stable than the RP phase.[37] However, Shang and co-workers used the DFT computation to show that the arene-based DJ phase has a higher dissociate energy and better kinetic stability than the RP phase.[38] Indeed, various works reported enhanced optical and humidity stabilities as the alkyl chain length increases in arene-based DJ phase perovskites[39–43] offering opportunities for the use of the DJ phase for optoelectronic applications.

The interlayer distance in layered halide perovskites has significant implications for the quantum and dielectric confinement effect.[44] In 2018, Ma and colleagues used a short propane-1,3-diammonium (PDA) cation to synthesize a (PDA)$MA_{n-1}Pb_nI_{3n+1}$ ($n = 2–4$) series layered perovskite.[45] It demonstrated the shortest interlayer distance of 2 Å in DJ phase perovskites. Huang and coauthors used transient photoluminescence mapping to visualize that the DJ phase perovskite not only confines the charge carrier in the in-plane direction but also becomes more conductive than the RP phase in the out-of-plane direction (Fig. 4b).[46] Thus, the DJ phase perovskite provides an expansive playground for more extensive photovoltaic and electronic application studies. While examples given in this section are mainly MA-based layered perovskites,[26] similar principles can be applied to FA-based DJ phase perovskites.
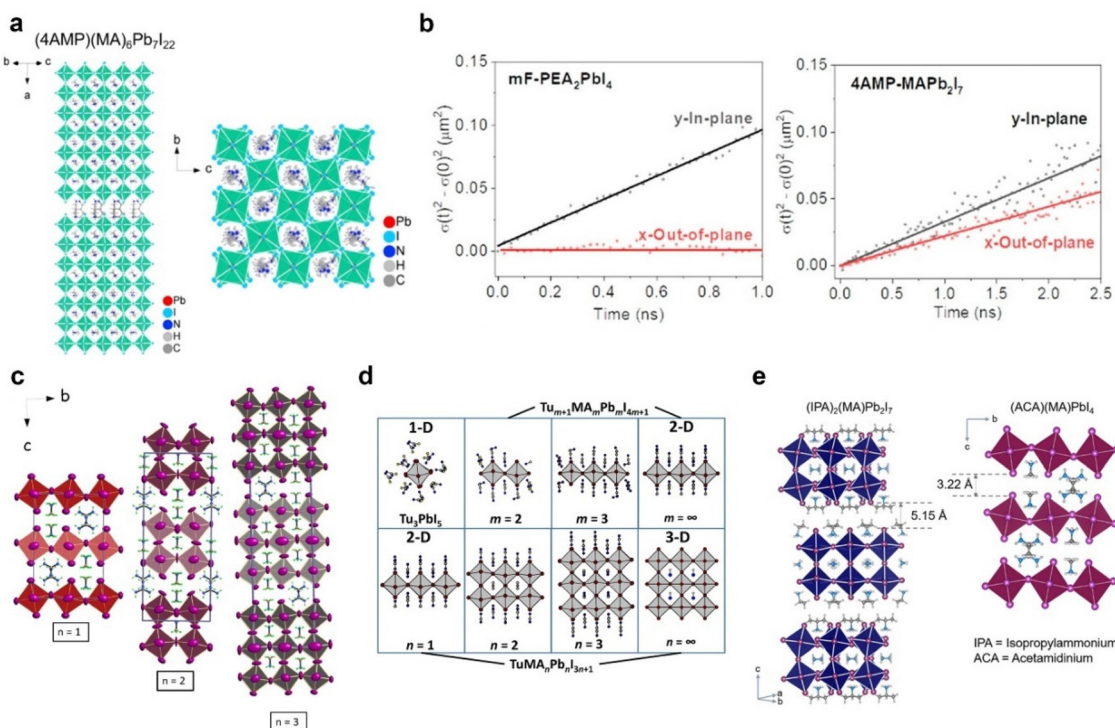
Fig. 4 Illustrations of some Dion–Jacobson (DJ) phase perovskites reported. (a) The crystal of $(4AMP)MA_6Pb_7I_{22}$ from the top-down and side views.[36] (b) Time-dependent mean-square distribution for photoluminescence emission spot broadening of RP and DJ phase perovskites along the in-plane and out-of-plane directions.[46] (c) Crystal structure of $(GA)(MA)_nPb_nI_{3n+1}$ ($n = 1–3$).[20] (d) Overview of the crystal structure of the TuI/MAI/PbI$_2$ system.[49] (e) Crystal structure of $(IPA)(MA)Pb_2I_7$ and $(ACA)(MA)PbI_4$.[50]

2.3 Alternating cations in the interlayer space (ACI) phase perovskites

The ACI phase combines the RP phase's chemical formation and the DJ phase's structural feature with the general formula of $AA'_nB_nX_{3n+1}$. The A-site cations include a small monocation (A' cation: Cs^+, MA^+, or FA^+) inside the perovskite cage and between the inorganic stacks alternating with a triammonium or diammonium cation (A cation) as spacers (Fig. 2c). The particular order leads to doubling of the unit cell along with the *b*-axis resulting in an ideal undistort cell. The inorganic layers demonstrate a (1/2, 0) offset along the *ab* plane, similar to the DJ phase perovskite. However, the interlayer sites differ from the DJ phase perovskite according to the charge balance restriction resulting in different centering of the unit cells. In 2017, Soe and colleagues used guanidinium (GA) to fabricate the first series of ACI phase $(GA)(MA)_nPb_nI_{3n+1}$ ($n = 1–3$) perovskite single crystals (Fig. 4c).[20] The optical property measurement of the $(GA)(MA)_nPb_nI_{3n+1}$ series shows a lower bandgap than that of the similar structure $BA_nMA_{n-1}Pb_nI_{3n+1}$ RP phase perovskites due to their smaller crystallographic distortion. Moreover, the $n = 3$ compound when applied as an active layer in a solar cell yielded a PCE of 7.3%. In 2019, Luo *et al.* used $(GA)(MA)_3Pb_3I_{10}$ as an active layer for solar cell demonstration, yielding a PCE of 18.5%.[47] Three years later, Zhang and colleagues used $(GA)(MA)_5Pb_5I_{16}$ to fabricate a highly efficient layered perovskite solar cell with a PCE of 22.3%.[48] In 2021, Daub *et al.* reported an analogous layered perovskite by using protonated thiourea (Tu^+) to synthesize $(Tu)(MA)PbI_4$ single crystals.[49] Its detailed crystal structure transition from 1D to 3D can be controlled by the chemical composition ratio (Fig. 4d). Recently, Mao and coworkers reported the ACI phase acetamidinium (ACA) perovskite single crystal, $(ACA)(MA)PbI_4$.[50] The interlayer distance is about 3.22 Å, which is more compact than that of the $(IPA)(MA)Pb_2I_7$ (separation distance of 5.15 Å) RP phase perovskite (Fig. 4e). As the separation distance decreased, the out-of-plane exciton transportation was improved, boosting the performance of the solar cell when the material was used. Zhu *et al.* reported two different chiral-polar hybrid ACI phase perovskite single crystals, $(MPA)(EA)PbBr_4$[51] and $(PPA)(EA)PbCl_4$.[52] Surprisingly, these two kinds of perovskites demonstrated self-powered circularly polarized light detection with high detectivity. It was the first realization of the chiral-polar photovoltaic effect in ACI phase perovskites. Even though ACI phase perovskites have been used in demonstrating solar cell devices, they were seldom applied in other semiconductor devices, such as light-emitting diodes or field-effect transistors possibly due to the limited diversity of ACI phase perovskites. Therefore, multiple research avenues exist to explore further new ACI phase perovskites and new properties for various semiconductor device applications.

3. Layered perovskite applications

There is an immense opportunity to apply layered metal halide perovskites for various semiconducting device applications. In 2021, the markets for solar cells, photodetectors, and field-effect transistors were worth around USD 91.6 billion, with a compound annual growth rate of 5–8%. Moreover, perovskite devices can be fabricated *via* a facile, solution-processed route, presenting potential upscaling advantages. In particular, the various crystallographic phases of layered metal halide perovskites (RP, DJ, and ACI phases) can be tailored for different device geometry designs. For example, DJ and ACI phase perovskites have lower exciton binding energy than the RP phase enabling vertical charge transport and are therefore more suitable for devices such as solar cells. On the other hand, RP phase perovskites present a better quantum confinement effect thus improving horizontal charge transport, making them more suitable than the other phases for planar geometry devices, such as field-effect transistors. This section will discuss the demonstrated applications of layered perovskites in optoelectronic devices.

3.1 Solar cell

While organic–inorganic hybrid perovskite solar cells are promising emerging thin film photovoltaic technology,[53] they are sensitive to moisture and heat, thus hindering their applications.[54] For example, a small amount of a Lewis base, such as water (from rain and humid air), can disrupt the hydrogen bond, coordinate with metal cations, and dissolve the perovskite material in 3D perovskites, along with other phase-induced changes causing degradation. As the water-induced decomposition process readily occurs due to the presence of volatile small organic cations, such as MA^+ and FA^+ in the A-site weakening non-covalent bonds between the organic and inorganic framework,[55] replacing these small and unstable hygroscopic organic cations with bulkier hydrophobic organic cations in the perovskite absorber layer in a solar device can improve its ambient stability. The absorber will inevitably be a lower-dimensional layered perovskite as the introduction of bulkier organic cations distorts the perovskite framework. Great progress has been made in layered perovskite solar cells with the PCE rapidly improving from 4.7% to 22.3% within only eight years (Fig. 5a).[47,48,56–61] Notable demonstrations including device structure and performance are listed in Table 1.

In 2014, Smith *et al.* demonstrated the first RP phase layered perovskite solar cells using $PEA_2MA_2Pb_3I_{10}$ ($PEA^+ = C_6H_5(CH_2)_2NH_3^+$).[56] The PCE was relatively low (4.7%) then, but the device demonstrated better moisture resistance than the control $MAPbI_3$ device. The relatively poor efficiency is due to the inhibition of vertical charge transport through the organic cation, which acted as an insulator between the conducting inorganic layers. In 2016, Tsai and colleagues overcame this issue by producing a near-single crystalline quality $BA_2MA_3Pb_4I_{13}$ ($BA^+ = CH_3(CH_2)_3NH_3^+$) thin film for a solar device producing a PCE of 12.5%. The un-encapsulated device also retained 60% of its initial PCE after 2250 hours of AM1.5G illumination with a relative humidity (RH) of 65%.[57] This breakthrough revived the interest in layered perovskite solar cells. Subsequently, Fu and co-authors introduced NH_4SCN and NH_4Cl additives into the $(PEA)_2MA_4Pb_5I_{16}$
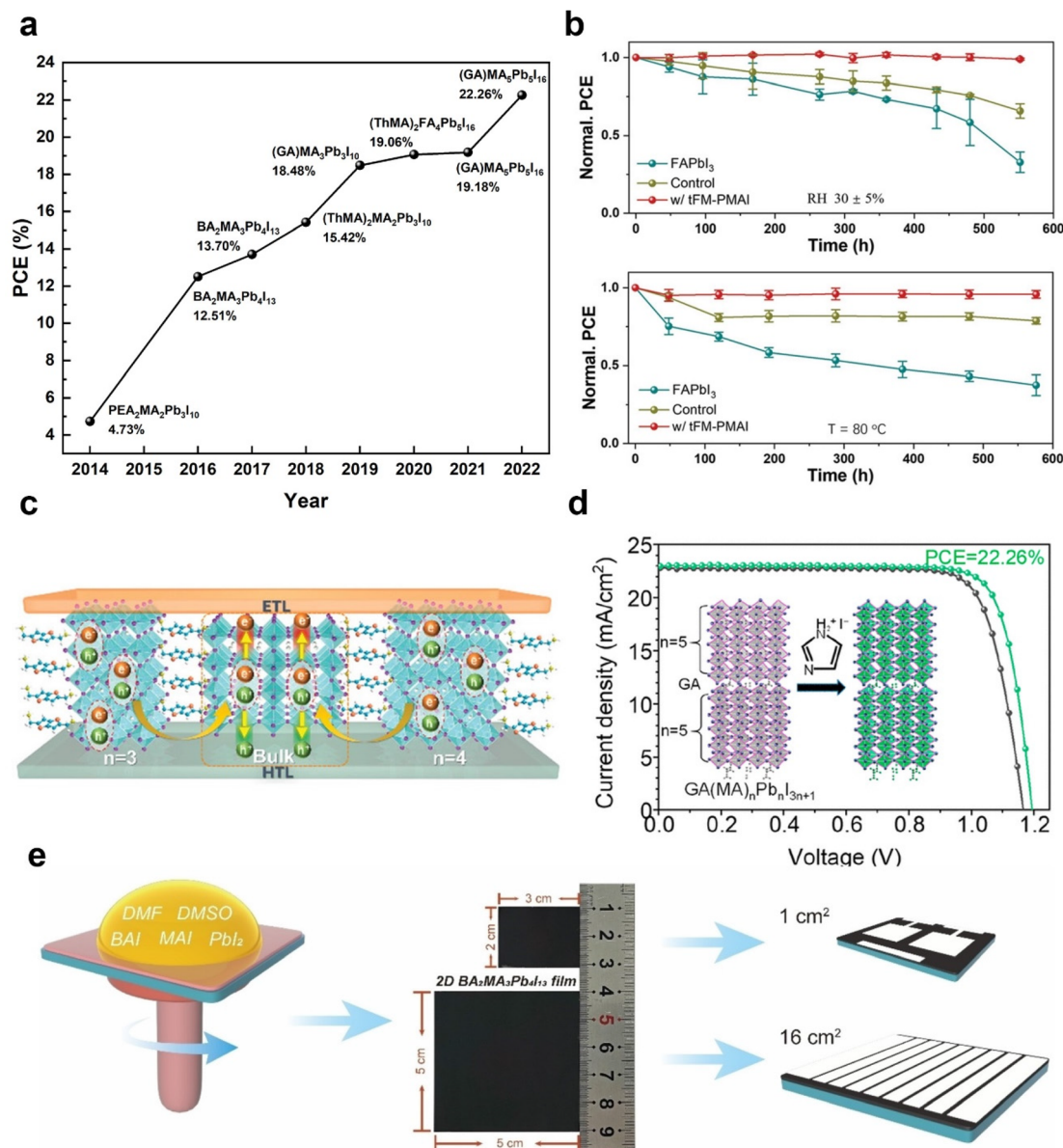
Fig. 5 Application of layered perovskites for photovoltaics. (a) PCE of notable layered perovskite solar cells from 2014 to 2022.[47,48,56–61] (b) Ambient and thermal stability measurements of a $(ThMA)_2FA_4Pb_5I_{16}$ perovskite solar cell.[60] (c) Illustration of the charge transfer of (TTDMA)$MA_{n-1}Pb_nI_{3n+1}$ film.[68] (d) Reverse and forward scanned J–V curves of ImI post-treated $(GA)(MA)_5Pb_5I_{16}$ perovskite solar cells with a PCE of 22.3%.[48] (e) Schematic diagram of a mini-module (5 × 5 cm^2) based on $BA_2MA_3Pb_4I_{13}$ perovskite solar cells.[69]

layered perovskite demonstrating a solar device with a best PCE of 14.1%.[62] The NH$_4$SCN additive was found to regulate the perovskite grain orientation enhancing crystallinity while the NH$_4$Cl additive passivated the interfacial traps between the electron transport layer and the perovskite layer.

In terms of layered perovskite crystallography, structural ordering of cation spacers can be induced by fluorine substitution in an aromatic cation spacer, such as PEA.[63] Zhang *et al.* used a *para*-position-fluorine-substituted PEA (F-PEA) to fabricate $(F\text{-}PEA)_2MA_2Pb_5I_{16}$ layered perovskite solar cells,[64] thus improving the best PCE from 9.7% to 13.6% after fluoride substitution due to the enhanced lifetime and lower trap

density of the perovskite layer. Furthermore, an un-encapsulated $(F\text{-}PEA)_2MA_2Pb_5I_{16}$ device maintained 65% of its initial PCE after 576 h at 70 °C. In the future, it may be possible to include the use of perfluoroarene-based cations[65] and their 1 : 1 mixtures with arene spacers (which went as far back as in 2003)[66] applicable to the DJ phase[67] for controlling the crystallographic characteristics and their associated properties for solar cell demonstrations.

In 2018, Lai and colleagues used 2-thiophenemethyl-ammonium (ThMA) cations as a spacer for $(ThMA)_2MA_2Pb_3I_{10}$ solar cell demonstration,[59] resulting in a PCE of 15.4% using the MACl assisted-film forming technique. Two years later, the same

Table 1 Performance layered perovskite solar cells

Materials	Device configuration	PCE (%)	PCE remained ratio (%)	RH (%)	Conditions	Times	Year
RP phase perovskites							
$PEA_2MA_3Pb_4I_{13}$[a]	FTO/PEDOT:PSS/perovskite/C_{60}/BCP/Ag[70]	18.5	90	40	Ambient	1200 h	2020
$(F\text{-}PEA)_2MA_2Pb_5I_{16}$[a]	FTO/c-TiO$_2$/perovskite/spiro-OMeTAD/Au[64]	13.6	65	N/A	Ambient, 70 °C	576 h	2019
$(F\text{-}PEA_{0.8}GA_{0.2})_2MA_3Pb_4I_{13}$[a]	ITO/PTAA/perovskite/C_{60}/BCP/Cu[71]	17.5	87	40–50	Ambient	500 h	2022
$BA_2MA_3Pb_4I_{13}$[a]	ITO/SnO$_2$/perovskite/spiro-OMeTAD/MoO$_3$/Au[72]	16.3	93.8	65 ± 10	Ambient	4680 h	2021
$BA_2MA_4Pb_5I_{16}$	ITO/PTAA/perovskite/C_{60}/BCP/Ag[73]	17.7	96.7	—	N$_2$	1000 h	2022
$BA_2MA_3Pb_4I_{13}$[a]	ITO/P3CT-BA/perovskite/PCBM/BCP/Ag[69]	17.6	90	40–50	Ambient, 20 °C	2400 h	2022
$(PA)_2MA_4Pb_5I_{16}$[a]	FTO/TiO$_2$/perovskite/spiro-OMeTAD/Au[74]	10.4	98	60	Ambient, 25 °C	500 h	2018
$(ThMA)_2MA_2Pb_3I_{10}$[a]	ITO/PEDOT:PSS/perovskite/PCBM/BCP/Ag[59]	15.4	90	30 ± 10	N$_2$	1000 h	2018
$(ThMA)_2FA_4Pb_5I_{16}$[a]	ITO/PEDOT:PSS/perovskite/PCBM/BCP/Ag[60]	19.1	99	30 ± 5	Ambient	552 h	2020
DJ phase perovskites							
$(3AMP)MA_3Pb_4I_{13}$	ITO/PEDOT:PSS/perovskite/C_{60}/BCP/Ag[19]	7.3	—	—	—	—	2018
$(4AMP)MA_3Pb_4I_{13}$	ITO/PEDOT:PSS/perovskite/C_{60}/BCP/Ag[19]	4.2	—	—	—	—	2018
$(PDMA)FA_2Pb_3I_{10}$[a]	FTO/c-TiO$_2$/m-TiO$_2$/perovskite/spiro-OMeTAD/Au[75]	6.9	85	30–50	Ambient	60 days	2018
$(PDA)MA_4Pb_4I_{13}$[a]	FTO/TiO$_2$/perovskite/spiro-OMeTAD/Au[76]	13.3	≥95	85	Ambient, 85 °C	168 h	2019
$(BDA)(Cs_{0.1}FA_{0.9})_4Pb_5I_{16}$[a]	FTO/c-TiO$_2$/m-TiO$_2$/perovskite/spiro-OMeTAD/Au[77]	18.2	90	35	Ambient, 35 °C	800 h	2020
$(TTDMA)MA_3Pb_4I_{13}$[a]	ITO/PEDOT:PSS/perovskite/PCBM/BCP/Ag[68]	18.8	≥99	—	N$_2$	4400 h	2021
ACI phase perovskites							
$GAMA_3Pb_3I_{10}$[a]	FTO/c-TiO$_2$/perovskite/PCBM/Ag[78]	14.1	88	30 ± 10	Ambient, 25 °C	240 days	2019
$GAMA_3Pb_3I_{10}$[a]	FTO/c-TiO$_2$/perovskite/PCBM/Ag[47]	18.5	95	30 ± 10	Ambient, 25 °C	131 days	2019
$GAMA_5Pb_5I_{16}$[a]	FTO/c-TiO$_2$/perovskite/spiro-OMeTAD/Au[61]	19.2	95	30 ± 10	Ambient, 25 °C	123 days	2021
$GAMA_5Pb_5I_{16}$	FTO/c-TiO$_2$/perovskite/spiro-OMeTAD/Au[48]	22.3	93.81	25	Ambient, 25 °C	50 days	2022

[a] Device without encapsulation.

group substituted the MA^+ cation with FA^+ to fabricate $(ThMA)_2FA_4Pb_5I_{16}$ solar cells with a PCE of 19.1%[60] and the unencapsulated device retained 99% of its initial PCE after 552 h of storage in ambient environment (RH = 30 ± 5%) or 96% of its initial PCE after 576 h of thermal annealing at 80 °C in N$_2$, respectively.

Due to lower exciton binding energy for vertical charge transport, DJ and ACI phase perovskite cells have recently outperformed their RP phase counterparts. In 2021, Xu *et al.* designed and synthesized a new type of fused-thiophene-based spacer, thieno[3,2-*b*]thiophene-2,5-diyldimethanaminium iodide (TTDMAI), for DJ phase perovskite solar cells.[68] TTDMAI provides a long π-conjugation chain and increasing grain size with vertical orientation due to the solid molecular interaction with the template. Thus, the exciton dissociation and charge transport were enhanced, as illustrated in Fig. 5c. The outstanding $(TTDMA)MA_3Pb_4I_{13}$ solar cell demonstrated a PCE of 18.8%. In 2022, Zhang *et al.* reported that the ACI phase $(GA)(MA)_5Pb_5I_{16}$ perovskite solar cells and amphoteric imidazolium iodide (ImI) post-treatment of the perovskite layer were responsible for boosting the outstanding device PCE to 22.3% (Fig. 5d).[48]

While large area solar cell demonstration using layered perovskites is still in its infancy at the time of writing of this review, in 2022, Han *et al.* reported the first 5 × 5 cm^2 layered perovskite solar cell mini-module (active area = 16 cm^2) based on $BA_2MA_3Pb_4I_{13}$ perovskites (Fig. 5e).[69] The best module PCE reached 11.1%, while the average was 10.5%. To date, no scalable processes, such as roll-to-roll, blade coating, or spray coating, have been applied to layered perovskite solar cells for module fabrication. Thus, there are opportunities for large area cell or module demonstrations using high-performance and more stable layered perovskites.

3.2 Photodetector

Photodetectors absorb light at a particular wavelength (range) of interest, and convert it into an electrical signal. The figures of merit, responsivity (R) and detectivity (D^*) are vital parameters for evaluating the performance of a photodetector. Responsivity refers to the net photocurrent generated from the incident light absorbed by the device in a unit of time. Detectivity reflects the capacity limit of a photodetector to detect low-intensity light. Layered metal halide perovskites are tunable in terms of light absorption wavelength range by changing the $[BX_6]^{4-}$ octahedra layer number between two adjacent spacers.[29] In addition, the inherent 2D quantum-confined structure in layered perovskites facilitates rapid photogenerated electron-hole pair dissociation which is more pronounced in RP-phase perovskites enabling rapid electron extraction to the inorganic conduction band with high carrier mobility reducing charge recombination and improving photoconductivity gains.[79] These unique properties of layered perovskites make them promising candidates for high-performance photodetectors. Some of the layered perovskite photodetectors reported are listed in Table 2.

In 2016, Zhou *et al.* demonstrated a $BA_2MA_{n-1}Pb_nI_{3n+1}$ (BA^+ = $C_4H_9NH_3^+$) thin-film-based perovskite photodetector with n = 1–3.[80] The layered perovskite exhibits an n-dependent absorbance spectrum and band diagram. The photoresponse corresponds to the inner perovskite layer thickness. Thus, the best performance was observed for larger n devices (Fig. 6a). In particular, the responsivity under 3.0 mW cm^{-2} white illumination for n = 1, 2, and 3 were 3.00, 7.31, and 12.78 mA W^{-1}, respectively. The relatively low responsivity was due to the presence of the insulating organic spacer acting as a charge barrier

Table 2 Performance of layered perovskite photodetectors

Materials	Morphology	Device fabrication	V_D (V)	R (A W^{-1})	D^*, light source (Jones, nm)	t_r/t_d	Year [ref.]
RP phase perovskites							
$(BA)_2(MA)_2Pb_3Br_{10}$	Single crystal	STL	5	—	3.6×10^{10}, 420	150/570 µs	2017 [89]
$Cs_2PbI_2Cl_2$	Single crystal	Solid-state method	10	—	—	0.2/0.06 s	2018 [33]
$(PEA)_2PbBr_4$	Single crystal	Evaporation process	10	3.148×10^{-2}	1.55×10^{13}, 365	0.41/0.37 ms	2019 [90]
$(PA)_2(GA)Pb_2I_7$	Single crystal	STL	10	47	6.3×10^{12}, 550	0.94/2.18 ns	2019 [83]
$(BPA)_2PbBr_4$	Single crystal	STL	0	10^{-4}	10^7, 377	27/30 µs	2020 [91]
$BDAPbI_4$	Single crystal	STL	10	9.27×10^{-1}	1.23×10^{11}, 462	187/163 µs	2020 [92]
$(BA)_2PbBr_4$	Single crystal film	AVC	4	4.5×10^{-2}	$\sim 1.02 \times 10^{12}$, 400	9.7/8.8 ms	2021 [93]
$Cs_2Pb(SCN)_2Br_2$	Single crystal	AVC	0.5	8.46×10^{-3}	1.2×10^{10}, 405	2.6/2.3 ms	2022 [34]
$(OA)_2(FA)_{n-1}Pb_nBr_{3n+1}$	Microplates	Drop-cast	9	32	—	0.25/1.45 ms	2017 [82]
$(BA)_2PbI_4$	Microplates	Solution-vapor method	5	—	—	58.8/56.6 ms	2018 [94]
$(PPA)_3Pb_2I_7$	Nanosheets	ASAC	—	—	1.2×10^{10}, 515	850/780 µs	2019 [95]
$(BA)_2(MA)_3Pb_4I_{13}$	Nanosheets	Inkjet-printed	40	0.17	3.7×10^{12}, 532	24/65 ms	2020 [96]
$(BA)_2(MA)Pb_2I_7$	Nanoplates	Drop-cast	10	4.5×10^{-3}	3.09×10^{10}, 550	<100 ms	2020 [97]
$(BA)_2(MA)_2Pb_3I_{10}$	Thin film	Spin coated	30	3×10^{-3}	—, white light	28.4/27.5 ms	2016 [80]
$(BA)_2(MA)Pb_2I_7$	Thin film	Spin coated	30	7.31×10^{-3}	—, white light	8.4/7.5 ms	2016 [80]
$(BA)_2PbI_4$	Thin film	Spin coated	30	1.278×10^{-2}	—, white light	10.0/7.5 ms	2016 [80]
$(BA)_2(MA)_3Pb_4I_{13}/IGZO$	Thin film	Spin coated	2	8.357×10^2	5.4×10^{12}, 520	128/647 ms	2022 [87]
$(iBA)_2(MA)_3Pb_4I_{13}$	Thin film	Hot-casted	1.5	1.171×10^{-1}	—, 532	16/15 ms	2018 [81]
DJ phase perovskites							
$(2meptH_2)(MA)Pb_2I_7$	Single crystal	STL	10	13	—, 405	40/— µs	2020 [98]
$(HDA)CsPb_2Br_7$	Single crystal	STL	10	8.2×10^{-5}	8.1×10^8, 405	200/300 µs	2020 [99]
$(4AMP)(MA)_2Pb_3Br_{10}/MAPbBr_3$	Single crystal	STL	0	1.19×10^{-3}	1.26×10^{12}, 405	600/600 µs	2020 [84]
$(EDA)(MA)Pb_2I_7$	Thin film	Spin coated	2	1.25×10^{-1}	7.1×10^{10}, 532	410/380 µs	2020 [100]
ACI phase perovskites							
$(GA)(FA)PbI_4$	Single crystal	STL	5	10^{-1}	2×10^{10}, 515	49/70 ms	2020 [101]
$(R\text{-}\beta\text{-}MPA)EAPbBr_4$	Single crystal	STL	0	—	1.1×10^{11}, 405	300/330 µs	2022 [51]
$(R\text{-}PPA)EACl_4$	Single crystal	STL	5	—	4.5×10^7, 266	—	2022 [52]

V_D, drain voltage; R, responsivity; D^*, specific detectivity; t_r/t_d, temporal response rise time/decay time; LDR, linear dynamic range.

and as a polycrystalline grain boundary, with both hindering charge carrier mobility. Therefore, Dong *et al.* substituted the BA$^+$ spacer with the branch i-BA$^+$ spacer for the fabrication of layered perovskites using a hot-casting method.[81] The responsivity of the $(iBA)_2(MA)_3Pb_4I_{13}$ photodetector significantly improved to 117.09 mA W^{-1} under a small bias voltage of 1.5 V. Moreover, rising and decay response speeds were significantly faster (about 16 and 15 ms, respectively). These improvements were attributed to the use of a shorter chain length branched spacer, a high-quality film with a larger grain size, and a reduced exciton binding energy in high *n*-value perovskites. However, stacked nano-sheets can result in interfacial charge carrier scattering and too much quantum confinement is undesirable. In fact, Yu *et al.* fabricated $OA_2FA_{n-1}Pb_nBr_{3n+1}$ (OA = octadecylamine) microplates with FA-acetate/acetic acid solution treatment to limit quantum confinement (Fig. 6b),[82] thereby (i) increasing 2D perovskite grain size *via* the partial exchange of OA$^+$ and FA$^+$ (ii) fusing 2D perovskite microplates forming integrated channels promoting charge carrier transport. Hence, the best demonstrated photodetector produced a very high responsivity of 32 A W^{-1} and reasonable response rise and decay times of 0.25 and 1.45 ms, respectively. In 2019, Xu and colleagues reported the first RP phase $(PA)_2(GA)Pb_2I_7$ perovskite single crystal[83] in which the GA$^+$ cations were confined in the cavity instead of the interlayer spacer (Fig. 6c). This provided a robust in-plane photoresponse, while the insulating PA$^+$ bilayer spacer performed as a hopping barrier to

effectively suppress the undesirable dark current ($\approx 2.4 \times 10^{-11}$ A). Therefore, the demonstrated single crystal photodetector produced a high responsivity and detectivity at 47 A W^{-1} and 6.3×10^{12} Jones, respectively.

In 2020, Zhang *et al.* demonstrated a 2D/3D heterostructured self-powered perovskite photodetector.[84] As shown in Fig. 6d, the heterostructured perovskite single crystal (4AMP) $(MA)_2Pb_3Br_{10}/MAPbBr_3$ was fabricated by tuning the molar compositions of 4-(aminomethyl)piperidinium bromide (4AMPBr$_2$), MABr, and PbBr$_2$. The device produced a high detectivity of 1.26×10^{12} Jones at zero bias which is compatible with those of BiFeO$_3$, MoS$_2$, and some of the state-of-the-art inorganic photodetectors.[85,86] Recently, Chen and colleagues integrated BA$_2$MA$_3$Pb$_4$I$_{13}$ with an IGZO thin film transistor (TFT) array demonstrating a phototransistor (Fig. 6e)[87] with a responsivity and detectivity of 835.7 A W^{-1} and 5.4×10^{12} Jones, respectively, under green light illumination. The BA$_2$MA$_3$Pb$_4$I$_{13}$/IGZO phototransistor array device was also capable of 64 pixels image detection recognizing the letters "S" and "Z". Even though the layered perovskite photodetectors (Table 2) have produced comparable responsivity and detectivity to those (~ 0.8 A W^{-1} and $\sim 10^{10}$ Jones) of state-of-the-art Si-based complementary metal–oxide–semiconductor (CMOS) devices,[88] they are still far from commercialization due to the insufficient integrated pixel number relative to commercial CMOS (6 megapixels with a device size of ~ 40 mm^2). The mass production of layered perovskite photodetectors may become a
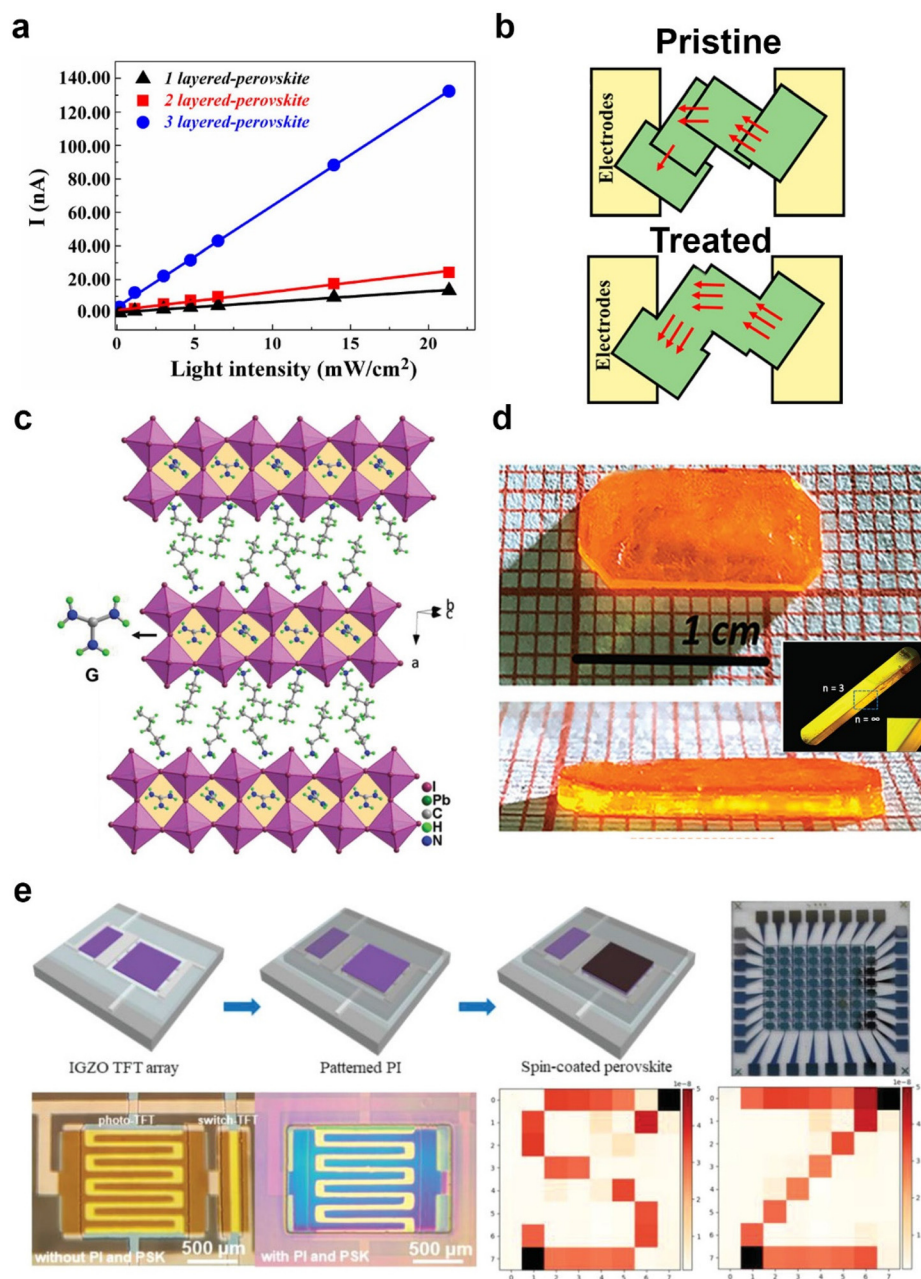
Fig. 6 Application of layered perovskites for photodetectors. (a) Photocurrent as a function of light intensity based on n values (1–3) for the $BA_2MA_{n-1}Pb_nI_{3n+1}$ photodetector with a V_b = 30 V.[80] (b) Illustration of the pristine and treated $(OA)_2(FA)_{n-1}Pb_nBr_{3n+1}$ microplate photodetector.[82] (c) The crystal structure of $(PA)_2(GA)Pb_2I_7$.[83] (d) Picture of $(4AMP)(MA)_2Pb_3I_{10}/MAPbBr_3$ heterostructure perovskite single crystal from the top and side views. Inset: optical microscopy image of the crystal boundary when n = 3 and n = ∞ and the (e) illustration and photos/optical microscope image of $BA_2MA_3Pb_4I_{13}$/IGZO TFT array at key fabrication steps. Mapping of the letter "S" and "Z" by the integrated 8 × 8 phototransistor array under illumination.[87]

challenge if they rely on custom-grown single crystals. Therefore, developing a scalable process for fabricating a high pixel integrated layered perovskite phototransistor will be relevant to potential commercialization.

3.3 Field effect transistor

A field-effect transistor (FET) is a widely used electronic device that controls current flow from the drain electrode to the source electrode under the influence of an applied electric field. The figures of merit, charge carrier (electron or hole) mobility and on/off ratio are vital parameters for evaluating the performance of a FET. The on/off ratio refers to the ratio between the "on" current and the "off"/"dark" current. The "on" state occurs when the gate voltage is larger than the threshold voltage (sufficient for conductivity in the channel between the source and the drain).[102] A high on/off ratio is

desired indicating effective drain and a low on/off ratio can be a sign of the presence of undesirable trap states due to low film quality. The current state-of-art inorganic transistors require deposition processes such as e-beam deposition and atomic layer deposition. Metal halide perovskite FETs may present cost advantages when fabricated by solution processes. Their ambipolar transport properties and high carrier mobilities are also desirable for FETs. In general, FET has four different configurations: top gate top contact (TGTC), top gate bottom contact (TGBC): bottom gate top contact (BGTC), and bottom gate bottom contact (BGBC) (Fig. 7). Typically, a bias voltage is applied to the gate and drain electrodes with the source electrode grounded during operation. In recent years, most of the perovskite thin film FETs have been fabricated in

the BGTC configuration due to their compatibility with the spin coating process while metal electrodes (source and drain) can be evaporated with no more subsequent solution processes. Due to the planar structure of the device, RP phase perovskites, such as PEA_2SnI_4, (Table 3) with better quantum confinement are more popular compared to the DJ and ACI phases for FET demonstrations due to better horizontal conductivity.

In 1999, the first layered perovskite PEA_2SnI_4 BGBC FET was reported by Kagan et al.[103] producing a saturation hole mobility of 0.62 cm^2 V^{-1} s^{-1} and an on/off ratio of 10^4 at room temperature indicating great potential of layered perovskite FETs. In 2002, Mitzi et al. demonstrated a melt-processed PEA_2SnI_4 BGBC FET.[104] The device was fabricated by placing
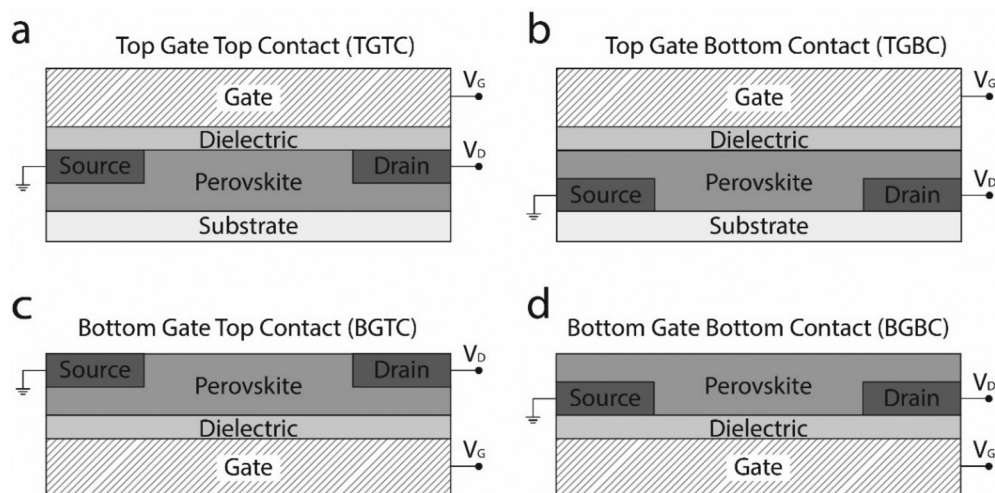

Fig. 7 Schematic of four different field-effect transistor device configurations. (a) Top gate top contact (TGTC), (b) top gate bottom contact (TGBC), (c) bottom gate top contact (BGTC), and (d) bottom gate bottom contact (BGBC).

Table 3 Performance of layered perovskite field-effect transistors at room temperature

Materials	Configuration	Dielectric layer	Drain and source	Mobility (cm^2 V^{-1} s^{-1}) Electrons	Holes	On/off ratio	Year [ref.]
PEA_2SnI_4	BGBC	SiO_2	Pd	—	0.62	10^4	1999 [103]
$(4\text{-}FPEA)_2SnI_4$	BGBC	SiO_2	Cr/Pd	—	0.2–0.6	$\approx 10^5$	2001 [109]
PEA_2SnI_4	BGBC	SiO_2	Pd	—	0.5	10^5	2001 [110]
PEA_2SnI_4	BGBC	SiO_2	Au	—	2.6	10^6	2002 [104]
PEA_2SnI_4	BGTC	SiO_2	Au	—	0.78	4.2×10^5	2004 [111]
PEA_2SnI_4	TGTC	Cytop	C_{60}/Al	1.5 ± 0.3	—	$(2.4 \pm 6.4) \times 10^4$	2016 [112]
PEA_2SnI_4	TGTC	Cytop	MoO_x/Au	—	12 ± 1	$(1.9 \pm 2.1) \times 10^6$	2016 [30]
PEA_2SnI_4	BGTC	SiO_2	Au	—	0.76–1.2	$> 10^3$	2017 [113]
$BA_2MA_2Pb_3I_{10}$	BGTC	SiO_2	Ag	1.25^a	—	$\approx 10^6$	2018 [105]
$(4Tm)_2SnI_4$	BGTC	SiO_2	Au	—	1.78	10^5–10^6	2019 [114]
PEA_2SnI_4	BGTC	PVA/CL-PVP	Au	—	0.30 ± 0.07	$\approx 10^3$	2019 [115]
PEA_2SnI_4	BGTC	SiO_2	Au	—	3.51 ± 0.60	3.4×10^6	2020 [106]
$BA_2MAPb_2I_7$	BGTC	SiO_2	Au	0.129 ± 0.048^a	—	10^6–10^7	2021 [116]
PEA_2SnI_4	BGTC	SiO_2	Au	—	2.03 ± 0.14	3.4×10^6	2021 [117]
TEA_2SnI_4	BGTC	SiO_2	Au	—	0.15	10^4	2022 [118]
PEA_2SnI_4	BGTC	SiO_2	Au	—	2.24	$\approx 10^6$	2022 [119]
PEA_2SnI_4 + 5 mol% SnF_2	BGBC	SiO_2	Au/Cr	—	0.68 ± 0.16	10^5	2022 [107]

^{a} Measured at 77 K for $BA_2MA_2Pb_3I_{10}$, and 150 K for $BA_2MAPb_2I_7$.

the PEA_2SnI_4 film between a polyimide-treated silicon wafer and a Kapton cover sheet (Fig. 8a) which was heated at 213 ± 5 °C (the melting point of PEA_2SnI_4), and then was further hand-pressed by another heated plate at a temperature 5–10 °C and above. After the melt-process treatment, the film morphology significantly improved with the enlarged grain size producing an enhanced hole mobility of about 2.6 cm^2 V^{-1} s^{-1} measured at room temperature. In 2018, Li and colleagues reported an n-type perovskite FET using $BA_2MA_{n-1}Pb_nI_{3n+1}$ (n = 1–3) single crystal flakes.[105] Device fabrication was done by exfoliating as-grown single crystals into flakes with a thickness of 80–100 nm with Scotch tape, which were then transferred onto a 285 nm-SiO_2-covered-Si substrate. The device produced a maximum electron mobility of 2×10^{-3}, 8.3×10^{-2}, and 1.25 cm^2 V^{-1} s^{-1} at n = 1, 2, and 3, respectively, at 77 K. Although the PL spectra blue shifts were observed to be indicative of phase transition (not shown here), no sudden increase or drop in mobility (Fig. 8b) was observed due to the transition that would other occur in 3D perovskites.

In 2020, Zhu *et al.* demonstrated a self-passivation method by using additional PEAI in PEA_2SnI_4 polycrystalline film.[106] Moreover, metallic Sn additive was added to the PEA_2SnI_4 pre-cursor to limit undesirable Sn oxidation. The combined benefits allowed the best FET to produce a hole mobility and on/off ratio of 3.51 ± 0.06 cm^2 V^{-1} s^{-1} and 3.4×10^6, respectively. In addition, the first perovskite-based complementary inverter was also demonstrated by combining an n-channel indium gallium zinc oxide (IGZO) FET with PEA_2SnI_4 BGTC FET (Fig. 8c). The inverter produced a high voltage gain of over 30 with low signal noise. Most recently, Liu *et al.* demonstrated a p-doped PEA_2SnI_4 BGBC FET device by adding SnF_4, improving hole mobility[107] from 0.25 ± 0.08 to 0.68 ± 0.16 cm^2 V^{-1} s^{-1} after adding 5 mol% SnF_2 additive. No further improvement but performance deterioration was observed when the SnF_2 concentration was further increased to 10 mol% (Fig. 8d).

While layered perovskite FETs have made outstanding progress in recent years (Table 3), there remain challenges and opportunities for further research and development. Firstly, there needs to be a rational design (*e.g.*, development of a model) for choosing the material for different layered perovskites for high-performance FETs. It will be most useful if material choice or the newly developed fabrication strategies can overcome the limited FET mobility demonstrated by the current layered perovskite which currently is well below those
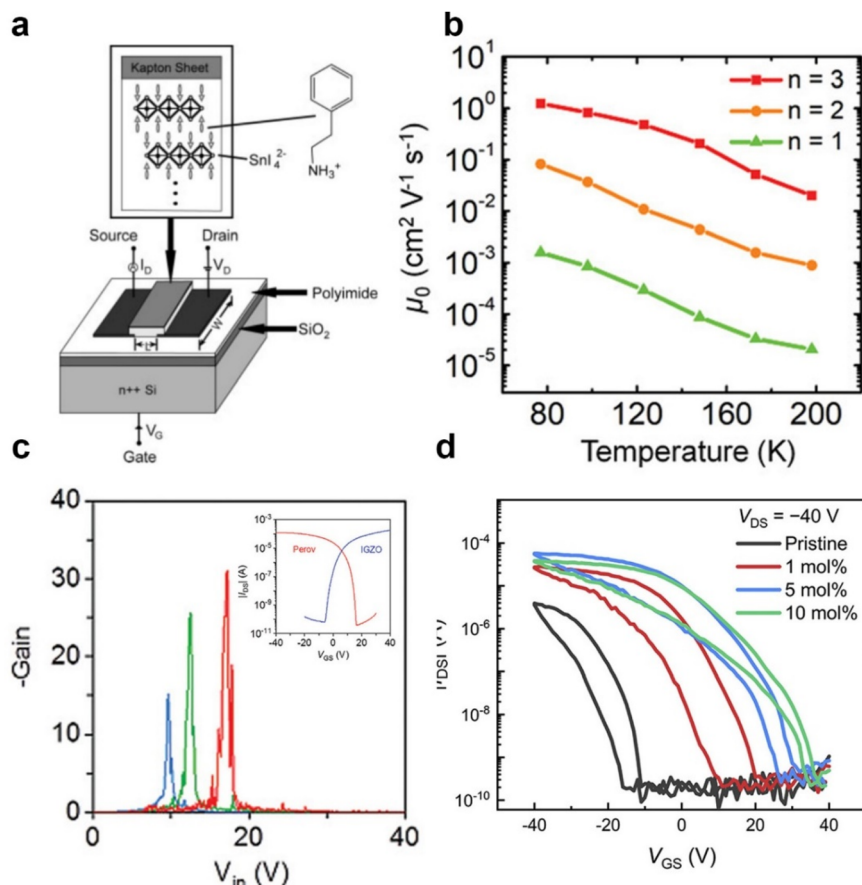

Fig. 8 Application of layered perovskites in field-effect transistors. (a) Illustration of melt-processed PEA_2SnI_4 FET on a silicon substrate. The inset illustrates the cross-section of the PEA_2SnI_4 and Kapton cover sheet.[103] (b) Measured mobility *versus* temperature of $BA_2MA_{n-1}Pb_nI_{3n+1}$ FET with different n (1, 2, and 3).[105] (c) Gain of the complementary PEA_2SnI_4/IGZO inverter at different direct voltage flows: at 20 (blue), 30 (green), and 40 (red) V. Inset: Transfer characteristics of a PEA_2SnI_4/IGZO inverter.[106] (d) Transfer characteristics of PEA_2SnI_4 with 0–10 mol% SnF_2 additives.[107]

of the state-of-arts, *e.g.*, 139.2 cm^2 V^{-1} s^{-1} for the best hydrogenated polycrystalline In$_2$O$_3$ (In$_2$O$_3$:H) FET.[108] While a layered perovskite FET is far from commercialization at this stage as device reliability and other manufacturing considerations such as scale up have not been seriously considered, there exist opportunities for further research such as the demonstration of perovskite FET array devices and integration of a perovskite FET with liquid crystal display (LCD), the most relevant application for thin film transistors.

4. Future outlook and conclusion

2D metal halide perovskites have immense potential for optoelectronic applications due to their enabling properties including enhanced stability and diverse choices in functional spacers and crystal phases such as the RP, DJ, and ACI phases. In this review, we have reviewed the rapid progress made for the applications of these phases in solar cells, photodetectors and field effect transistors (FET), and there remain opportunities and challenges requiring further research and development (R&D).

In terms of solar cells using layered perovskites as absorbers, R&D opportunities include: (i) interface and interlayer optimization by a surface passivation layer and development of a self-assembled monolayer for a charge selective layer; (ii) the use of layered perovskites for high and low bandgap solar cells for multi-junction tandem solar cells; and (iii) the development of scalable processes for layered perovskites for large areas or module demonstrations. In addition, we need a better understanding of the real material composition, stoichiometry, presence of gradient rather than pure phases, and grain orientations. Current reports so far rely on nominal concentrations of precursor components for material identification which is limiting. A deeper understanding of the material structure of layered perovskites will enable better engineering to enhance the functionality of spacer cations[120,121] to improve the performance of not just solar cells but also photodetectors and FETs.

For photodetectors, a new pixel-integrated method compatible with layered perovskites needs to be developed as the current industry method *via* molecular beam epitaxy for the traditional Ge photodetector on a silicon circuit is not compatible with metal halide perovskites. Further work can also be done on achieving better band alignment between the layered perovskite and metal electrode for better charge extraction. In terms of challenges, instability (from halogen ion reactions with metal electrodes forming metal halides (AgI$_2$, CuI$_2$, or AuI$_2$)) under a bias voltage (typically 1–10 V) needs to be overcome. This not only impacts photodetectors but also FETs, perhaps more severely due to the higher operational bias (*e.g.*, 10–60 V for typical drain voltage).

For FETs, it will be beneficial for developing a rational material design (*e.g.*, development of models predicting electronic properties that are also relevant to specific FET device operation mechanisms) to expand layered perovskite choices other than the popular PEA$_2$SnI$_4$ at present. There is also an urgent need to improve layered perovskite FET mobility to reach parity with the state-of-the-art thin film transistor (TFT) devices.

Conflicts of interest

There are no conflicts to declare.

Acknowledgements

References

1 M. V. Kovalenko, L. Protesescu and M. I. Bodnarchuk, Properties and potential optoelectronic applications of lead halide perovskite nanocrystals, *Science*, 2017, **358**(6364), 745.

2 J. Pan, L. N. Quan, Y. Zhao, W. Peng, B. Murali, S. P. Sarmah, M. Yuan, L. Sinatra, N. M. Alyami and J. Liu, Highly efficient perovskite-quantum-dot light-emitting diodes by surface engineering, *Adv. Mater.*, 2016, **28**(39), 8718.

3 S. D. Stranks, G. E. Eperon, G. Grancini, C. Menelaou, M. J. Alcocer, T. Leijtens, L. M. Herz, A. Petrozza and H. J. Snaith, Electron-hole diffusion lengths exceeding 1 micrometer in an organometal trihalide perovskite absorber, *Science*, 2013, **342**(6156), 341.

4 J. H. Noh, S. H. Im, J. H. Heo, T. N. Mandal and S. I. Seok, Chemical management for colorful, efficient, and stable inorganic–organic hybrid nanostructured solar cells, *Nano Lett.*, 2013, **13**(4), 1764.

5 F. Hao, C. C. Stoumpos, D. H. Cao, R. P. Chang and M. G. Kanatzidis, Lead-free solid-state organic–inorganic halide perovskite solar cells, *Nat. Photonics*, 2014, **8**(6), 489.

6 M. A. Green, A. Ho-Baillie and H. J. Snaith, The emergence of perovskite solar cells, *Nat. Photonics*, 2014, **8**(7), 506.

7 R. P. Sabatini, C. Liao, S. Bernardi, W. Mao, M. S. Rahme, A. Widmer-Cooper, U. Bach, S. Huang, A. W. Ho-Baillie and G. Lakhwani, Solution-Processed Faraday Rotators Using Single Crystal Lead Halide Perovskites, *Adv. Sci.*, 2020, **7**(7), 1902950.

8 A. Kojima, K. Teshima, Y. Shirai and T. Miyasaka, Organometal halide perovskites as visible-light sensitizers for photovoltaic cells, *J. Am. Chem. Soc.*, 2009, **131**(17), 6050.

9 National Renewable Energy Laboratory, Best Research-Cell Efficiency Chart, 2022, https://www.nrel.gov/pv/assets/pdfs/best-research-cell-efficiencies-rev220630.pdf.

10 S. Yakunin, L. Protesescu, F. Krieg, M. I. Bodnarchuk, G. Nedelcu, M. Humer, G. De Luca, M. Fiebig, W. Heiss and M. V. Kovalenko, Low-threshold amplified spontaneous emission and lasing from colloidal nanocrystals of caesium lead halide perovskites, *Nat. Commun.*, 2015, **6**(1), 1.

11 Y. Zou, H. Y. Wang, Y. Qin, C. Mu, Q. Li, D. Xu and J. P. Zhang, Reduced Defects of $MAPbI_3$ Thin Films Treated by FAI for High-Performance Planar Perovskite Solar Cells, *Adv. Funct. Mater.*, 2019, **29**(7), 1805810.

12 P. V. Chandrasekar, S. Yang, J. Hu, M. Sulaman, Y. Shi, M. I. Saleem, Y. Tang, Y. Jiang and B. Zou, Solution-phase, template-free synthesis of PbI_2 and $MAPbI_3$ nano/micro-tubes for high-sensitivity photodetectors, *Nanoscale*, 2019, **11**(12), 5188.

13 W. Yu, F. Li, L. Yu, M. R. Niazi, Y. Zou, D. Corzo, A. Basu, C. Ma, S. Dey and M. L. Tietze, Single crystal hybrid perovskite field-effect transistors, *Nat. Commun.*, 2018, **9**(1), 1.

14 S. P. Senanayak, M. Abdi-Jalebi, V. S. Kamboj, R. Carey, R. Shivanna, T. Tian, G. Schweicher, J. Wang, N. Giesbrecht and D. Di Nuzzo, A general approach for hysteresis-free, operationally stable metal halide perovskite field-effect transistors, *Sci. Adv.*, 2020, **6**(15), eaaz4948.

15 V. M. Goldschmidt, Die gesetze der krystallochemie, *Naturwissenschaften*, 1926, **14**(21), 477.

16 L. Mao, Y. Wu, C. C. Stoumpos, B. Traore, C. Katan, J. Even, M. R. Wasielewski and M. G. Kanatzidis, Tunable White-Light Emission in Single-Cation-Templated Three-Layered 2D Perovskites $(CH_3CH_2NH_3)_4Pb_3Br_{10-x}Cl_x$, *J. Am. Chem. Soc.*, 2017, **139**(34), 11956.

17 E. I. Marchenko, S. A. Fateev, A. A. Petrov, V. V. Korolev, A. Mitrofanov, A. V. Petrov, E. A. Goodilin and A. B. Tarasov, Database of two-dimensional hybrid perovskite materials: open-access collection of crystal structures, band gaps, and atomic partial charges predicted by machine learning, *Chem. Mater.*, 2020, **32**(17), 7383.

18 S. Ruddlesden and P. Popper, The compound $Sr_3Ti_2O_7$ and its structure, *Acta Crystallogr.*, 1958, **11**(1), 54.

19 L. Mao, W. Ke, L. Pedesseau, Y. Wu, C. Katan, J. Even, M. R. Wasielewski, C. C. Stoumpos and M. G. Kanatzidis, Hybrid Dion–Jacobson 2D lead iodide perovskites, *J. Am. Chem. Soc.*, 2018, **140**(10), 3775.

20 C. M. M. Soe, C. C. Stoumpos, M. Kepenekian, B. Traoré, H. Tsai, W. Nie, B. Wang, C. Katan, R. Seshadri and A. D. Mohite, New type of 2D perovskites with alternating cations in the interlayer space, $(C(NH_2)_3)(CH_3NH_3)_nPb_nI_{3n+1}$: Structure, properties, and photovoltaic performance, *J. Am. Chem. Soc.*, 2017, **139**(45), 16297.

21 X. Li, J. M. Hoffman and M. G. Kanatzidis, The 2D halide perovskite rulebook: how the spacer influences everything from the structure to optoelectronic device efficiency, *Chem. Rev.*, 2021, **121**(4), 2230.

22 J.-C. Blancon, A. V. Stier, H. Tsai, W. Nie, C. C. Stoumpos, B. Traore, L. Pedessseau, M. Kepenekian, F. Katsutani and G. Noe, Scaling law for excitons in 2D perovskite quantum wells, *Nat. Commun.*, 2018, **9**(1), 1.

23 D. B. Mitzi, C. Feild, W. Harrison and A. Guloy, Conducting tin halides with a layered organic-based perovskite structure, *Nature*, 1994, **369**(6480), 467.

24 D. T. Gangadharan and D. Ma, Searching for stability at lower dimensions: current trends and future prospects of layered perovskite solar cells, *Energy Environ. Sci.*, 2019, **12**(10), 2860.

25 C. M. M. Soe, G. Nagabhushana, R. Shivaramaiah, H. Tsai, W. Nie, J.-C. Blancon, F. Melkonyan, D. H. Cao, B. Traoré and L. Pedessseau, Structural and thermodynamic limits of layer thickness in 2D halide perovskites, *Proc. Natl. Acad. Sci. U. S. A.*, 2019, **116**(1), 58.

26 J. V. Milić, S. M. Zakeeruddin and M. Grätzel, Layered hybrid formamidinium lead iodide perovskites: challenges and opportunities, *Acc. Chem. Res.*, 2021, **54**(12), 2729.

27 G. Wu, X. Li, J. Zhou, J. Zhang, X. Zhang, X. Leng, P. Wang, M. Chen, D. Zhang and K. Zhao, Fine multi-phase Alignments in 2D perovskite solar cells with efficiency over 17% via slow post-annealing, *Adv. Mater.*, 2019, **31**(42), 1903889.

28 H. Tsai, W. Nie, J. C. Blancon, C. C. Stoumpos, C. M. M. Soe, J. Yoo, J. Crochet, S. Tretiak, J. Even and A. Sadhanala, Stable light-emitting diodes using phase-pure Ruddlesden–Popper layered perovskites, *Adv. Mater.*, 2018, **30**(6), 1704217.

29 Z. Tan, Y. Wu, H. Hong, J. Yin, J. Zhang, L. Lin, M. Wang, X. Sun, L. Sun and Y. Huang, Two-dimensional $(C_4H_9NH_3)_2PbBr_4$ perovskite crystals for high-performance photodetector, *J. Am. Chem. Soc.*, 2016, **138**(51), 16612.

30 T. Matsushima, S. Hwang, A. S. Sandanayaka, C. Qin, S. Terakawa, T. Fujihara, M. Yahiro and C. Adachi, Solution-processed organic–inorganic perovskite field-effect transistors with high hole mobilities, *Adv. Mater.*, 2016, **28**(46), 10275.

31 B. Walker, G. H. Kim and J. Y. Kim, Pseudohalides in lead-based perovskite semiconductors, *Adv. Mater.*, 2019, **31**(20), 1807029.

32 M. Daub and H. Hillebrecht, Synthesis, Single-Crystal Structure and Characterization of $(CH_3NH_3)_2Pb(SCN)_2I_2$, *Angew. Chem.*, 2015, **127**(38), 11168.

33 J. Li, Q. Yu, Y. He, C. C. Stoumpos, G. Niu, G. G. Trimarchi, H. Guo, G. Dong, D. Wang and L. Wang, $Cs_2PbI_2Cl_2$, all-inorganic two-dimensional Ruddlesden–Popper mixed halide perovskite with optoelectronic response, *J. Am. Chem. Soc.*, 2018, **140**(35), 11085.

34 C. H. Liao, C. H. Chen, J. Bing, C. Bailey, Y. T. Lin, T. M. Pandit, L. Granados, J. Zheng, S. Tang, B. H. Lin, *et al.*, Inorganic-Cation Pseudohalide 2D $Cs_2Pb(SCN)_2Br_2$ Perovskite Single Crystal, *Adv. Mater.*, 2022, **34**(7), 2104782.

35 N. Mercier, Hybrid halide perovskites: Discussions on terminology and materials, *Angew. Chem., Int. Ed.*, 2019, **58**(50), 17912.

36 L. Mao, R. M. Kennard, B. Traore, W. Ke, C. Katan, J. Even, M. L. Chabinyc, C. C. Stoumpos and M. G. Kanatzidis, Seven-layered 2D hybrid lead iodide perovskites, *Chem*, 2019, **5**(10), 2593.

37 E. S. Vasileiadou, B. Wang, I. Spanopoulos, I. Hadar, A. Navrotsky and M. G. Kanatzidis, Insight on the stability of thick layers in 2D Ruddlesden–Popper and Dion–Jacobson lead iodide perovskites, *J. Am. Chem. Soc.*, 2021, **143**(6), 2523.

38 Y. Shang, Y. Liao, Q. Wei, Z. Wang, B. Xiang, Y. Ke, W. Liu and Z. Ning, Highly stable hybrid perovskite light-emitting diodes based on Dion-Jacobson structure, *Sci. Adv.*, 2019, **5**(8), eaaw8072.

39 Y. Li, J. V. Milić, A. Ummadisingu, J.-Y. Seo, J.-H. Im, H.-S. Kim, Y. Liu, M. I. Dar, S. M. Zakeeruddin, P. Wang, *et al.*, Bifunctional organic spacers for formamidinium-based hybrid Dion–Jacobson two-dimensional perovskite solar cells, *Nano Lett.*, 2018, **19**(1), 150.

40 A. Dučinskas, G. Y. Kim, D. Moia, A. Senocrate, Y.-R. Wang, M. A. Hope, A. Mishra, D. J. Kubicki, M. Siczek, W. Bury, *et al.*, Unravelling the Behavior of Dion–Jacobson Layered Hybrid Perovskites in Humid Environments, *ACS Energy Lett.*, 2020, **6**(2), 337.

41 A. Dučinskas, G. C. Fish, M. A. Hope, L. Merten, D. Moia, A. Hinderhofer, L. C. Carbone, J.-E. Moser, F. Schreiber, J. Maier, *et al.*, The Role of Alkyl Chain Length and Halide Counter Ion in Layered Dion–Jacobson Perovskites with Aromatic Spacers, *J. Phys. Chem. Lett.*, 2021, **12**(42), 10325.

42 B.-E. Cohen, Y. Li, Q. Meng and L. Etgar, Dion–Jacobson two-dimensional perovskite solar cells based on benzene dimethanammonium cation, *Nano Lett.*, 2019, **19**(4), 2588.

43 A. Ummadisingu, A. Mishra, D. J. Kubicki, T. LaGrange, A. Dučinskas, M. Siczek, W. Bury, J. V. Milić, M. Grätzel and L. Emsley, Multi-Length Scale Structure of 2D/3D Dion–Jacobson Hybrid Perovskites Based on an Aromatic Diammonium Spacer, *Small*, 2022, **18**(5), 2104287.

44 C. Katan, N. Mercier and J. Even, Quantum and dielectric confinement effects in lower-dimensional hybrid perovskite semiconductors, *Chem. Rev.*, 2019, **119**(5), 3140.

45 C. Ma, D. Shen, T. W. Ng, M. F. Lo and C. S. Lee, 2D perovskites with short interlayer distance for high-performance solar cell application, *Adv. Mater.*, 2018, **30**(22), 1800710.

46 Z. Shi, Z. Ni and J. Huang, Direct Observation of Fast Carriers Transport along Out-of-Plane Direction in a Dion–Jacobson Layered Perovskite, *ACS Energy Lett.*, 2022, **7**(3), 984.

47 T. Luo, Y. Zhang, Z. Xu, T. Niu, J. Wen, J. Lu, S. Jin, S. Liu and K. Zhao, Compositional control in 2D perovskites with alternating cations in the interlayer space for photovoltaics with efficiency over 18%, *Adv. Mater.*, 2019, **31**(44), 1903848.

48 Y. Zhang and N.-G. Park, Quasi-Two-Dimensional Perovskite Solar Cells with Efficiency Exceeding 22%, *ACS Energy Lett.*, 2022, **7**(2), 757.

49 M. Daub and H. Hillebrecht, From 1D to 3D: Perovskites within the system HSC(NH$_2$)$_2$I/CH$_3$NH$_3$I/PbI$_2$ with maintenance of the cubic closest packing, *Inorg. Chem.*, 2021, **60**(5), 3082.

50 L. Mao, E. E. Morgan, A. Li, R. M. Kennard, M. J. Hong, Y. Liu, C. J. Dahlman, J. G. Labram, M. L. Chabinyc and R. Seshadri, Layered Hybrid Lead Iodide Perovskites with Short Interlayer Distances, *ACS Energy Lett.*, 2022, **7**(8), 2801.

51 W. Wu, L. Li, D. Li, Y. Yao, Z. Xu, X. Liu, M. Hong and J. Luo, Tailoring the Distinctive Chiral-Polar Perovskites with Alternating Cations in the Interlayer Space for Self-Driven Circularly Polarized Light Detection, *Adv. Opt. Mater.*, 2022, 2102678.

52 T. Zhu, H. Wu, C. Ji, X. Zhang, Y. Peng, Y. Yao, H. Ye, W. Weng, W. Lin and J. Luo, Polar Photovoltaic Effect in Chiral Alternating Cations Intercalation-Type Perovskites Driving Self-Powered Ultraviolet Circularly Polarized Light Detection, *Adv. Opt. Mater.*, 2022, **10**(15), 2200146.

53 O. Almora, D. Baran, G. C. Bazan, C. I. Cabrera, S. Erten-Ela, K. Forberich, F. Guo, J. Hauch, A. W. Y. Ho-Baillie, T. J. Jacobsson, *et al.*, Device Performance of Emerging Photovoltaic Materials (Version 3), *Adv. Energy Mater.*, 2023, **13**(1), 2203313.

54 A. M. Leguy, Y. Hu, M. Campoy-Quiles, M. I. Alonso, O. J. Weber, P. Azarhoosh, M. Van Schilfgaarde, M. T. Weller, T. Bein and J. Nelson, Reversible hydration of CH$_3$NH$_3$PbI$_3$ in films, single crystals, and solar cells, *Chem. Mater.*, 2015, **27**(9), 3397.

55 Z. Xiao, D. Wang, Q. Dong, Q. Wang, W. Wei, J. Dai, X. Zeng and J. Huang, Unraveling the hidden function of a stabilizer in a precursor in improving hybrid perovskite film morphology for high efficiency solar cells, *Energy Environ. Sci.*, 2016, **9**(3), 867.

56 I. C. Smith, E. T. Hoke, D. Solis-Ibarra, M. D. McGehee and H. I. Karunadasa, A layered hybrid perovskite solar-cell absorber with enhanced moisture stability, *Angew. Chem., Int. Ed.*, 2014, **53**(42), 11232.

57 H. Tsai, W. Nie, J.-C. Blancon, C. C. Stoumpos, R. Asadpour, B. Harutyunyan, A. J. Neukirch, R. Verduzco, J. J. Crochet, S. Tretiak, *et al.*, High-efficiency two-dimensional Ruddlesden–Popper perovskite solar cells, *Nature*, 2016, **536**(7616), 312.

58 X. Zhang, X. Ren, B. Liu, R. Munir, X. Zhu, D. Yang, J. Li, Y. Liu, D.-M. Smilgies and R. Li, Stable high efficiency two-dimensional perovskite solar cells via cesium doping, *Energy Environ. Sci.*, 2017, **10**(10), 2095.

59 H. Lai, B. Kan, T. Liu, N. Zheng, Z. Xie, T. Zhou, X. Wan, X. Zhang, Y. Liu and Y. Chen, Two-dimensional Ruddlesden–Popper perovskite with nanorod-like morphology for solar cells with efficiency exceeding 15%, *J. Am. Chem. Soc.*, 2018, **140**(37), 11639.

60 H. Lai, D. Lu, Z. Xu, N. Zheng, Z. Xie and Y. Liu, Organic-Salt-Assisted Crystal Growth and Orientation of Quasi-2D Ruddlesden–Popper Perovskites for Solar Cells with Efficiency over 19%, *Adv. Mater.*, 2020, **32**(33), 2001470.

61 J. Yang, T. Yang, D. Liu, Y. Zhang, T. Luo, J. Lu, J. Fang, J. Wen, Z. Deng and S. Liu, Stable 2D Alternating Cation Perovskite Solar Cells with Power Conversion Efficiency >19% via Solvent Engineering, *Sol. RRL*, 2021, **5**(8), 2100286.

62 W. Fu, J. Wang, L. Zuo, K. Gao, F. Liu, D. S. Ginger and A. K.-Y. Jen, Two-dimensional perovskite solar cells with 14.1% power conversion efficiency and 0.68% external radiative efficiency, *ACS Energy Lett.*, 2018, **3**(9), 2086.

63 J. Hu, I. W. Oswald, S. J. Stuard, M. M. Nahid, N. Zhou, O. F. Williams, Z. Guo, L. Yan, H. Hu and Z. Chen, Synthetic control over orientational degeneracy of spacer cations enhances solar cell efficiency in two-dimensional perovskites, *Nat. Commun.*, 2019, **10**(1), 1.

64 F. Zhang, D. H. Kim, H. Lu, J.-S. Park, B. W. Larson, J. Hu, L. Gao, C. Xiao, O. G. Reid and X. Chen, Enhanced charge transport in 2D perovskites via fluorination of organic cation, *J. Am. Chem. Soc.*, 2019, **141**(14), 5972.

65 J. V. Milić, Perfluoroarenes: A Versatile Platform for Hybrid Perovskite Photovoltaics, *J. Phys. Chem. Lett.*, 2022, **13**(42), 9869.

66 Z. Xu and D. B. Mitzi, SnI_4^{2-}-based hybrid perovskites templated by multiple organic cations: Combining organic functionalities through noncovalent interactions, *Chem. Mater.*, 2003, **15**(19), 3632.

67 M. Almalki, A. Dučinskas, L. C. Carbone, L. Pfeifer, L. Piveteau, W. Luo, E. Lim, P. A. Gaina, P. A. Schouwink and S. M. Zakeeruddin, Nanosegregation in arene-perfluoroarene π-systems for hybrid layered Dion–Jacobson perovskites, *Nanoscale*, 2022, **14**, 6771–6776.

68 Z. Xu, D. Lu, X. Dong, M. Chen, Q. Fu and Y. Liu, Highly Efficient and Stable Dion–Jacobson Perovskite Solar Cells Enabled by Extended π-Conjugation of Organic Spacer, *Adv. Mater.*, 2021, **33**(51), 2105083.

69 C. Han, Y. Wang, J. Yuan, J. Sun, X. Zhang, C. Cazorla, X. Wu, Z. Wu, J. Shi and J. Guo, Tailoring Phase Alignment and Interfaces via Polyelectrolyte Anchoring Enables Large-Area 2D Perovskite Solar Cells, *Angew. Chem., Int. Ed.*, 2022, **61**(36), e202205111.

70 Y. Yang, C. Liu, O. A. Syzgantseva, M. A. Syzgantseva, S. Ma, Y. Ding, M. Cai, X. Liu, S. Dai and M. K. Nazeeruddin, Defect suppression in oriented 2D perovskite solar cells with efficiency over 18% via rerouting crystallization pathway, *Adv. Energy Mater.*, 2021, **11**(1), 2002966.

71 J. Xu, J. Chen, S. Chen, H. Gao, Y. Li, Z. Jiang, Y. Zhang, X. Wang, X. Zhu and B. Xu, Organic Spacer Engineering of Ruddlesden-Popper Perovskite Materials toward Efficient and Stable Solar Cells, *Chem. Eng. J.*, 2022, 139790, DOI: **10.1016/j.cej.2022.139790**.

72 C. Liang, H. Gu, Y. Xia, Z. Wang, X. Liu, J. Xia, S. Zuo, Y. Hu, X. Gao and W. Hui, Two-dimensional Ruddlesden–Popper layered perovskite solar cells based on phase-pure thin films, *Nat. Energy*, 2021, **6**(1), 38.

73 H. Wang, Y. Pan, X. Li, Z. Shi, X. Zhang, T. Shen, Y. Tang, W. Fan, Y. Zhang and F. Liu, Band Alignment Boosts over 17% Efficiency Quasi-2D Perovskite Solar Cells via Bottom-Side Phase Manipulation, *ACS Energy Lett.*, 2022, **7**, 3187.

74 P. Cheng, Z. Xu, J. Li, Y. Liu, Y. Fan, L. Yu, D.-M. Smilgies, C. Müller, K. Zhao and S. F. Liu, Highly efficient Ruddlesden–Popper halide perovskite $PA_2MA_4Pb_5I_{16}$ solar cells, *ACS Energy Lett.*, 2018, **3**(8), 1975.

75 Y. Li, J. V. Milić, A. Ummadisingu, J.-Y. Seo, J.-H. Im, H.-S. Kim, Y. Liu, M. I. Dar, S. M. Zakeeruddin and P. Wang, Bifunctional organic spacers for formamidinium-based hybrid Dion–Jacobson two-dimensional perovskite solar cells, *Nano Lett.*, 2018, **19**(1), 150.

76 S. Ahmad, P. Fu, S. Yu, Q. Yang, X. Liu, X. Wang, X. Wang, X. Guo and C. Li, Dion-Jacobson phase 2D layered perovskites for solar cells with ultrahigh stability, *Joule*, 2019, **3**(3), 794.

77 X. Zhao, T. Liu, A. B. Kaplan, C. Yao and Y.-L. Loo, Accessing highly oriented two-dimensional perovskite films via solvent-vapor annealing for efficient and stable solar cells, *Nano Lett.*, 2020, **20**(12), 8880.

78 Y. Zhang, P. Wang, M.-C. Tang, D. Barrit, W. Ke, J. Liu, T. Luo, Y. Liu, T. Niu and D.-M. Smilgies, Dynamical transformation of two-dimensional perovskites with alternating cations in the interlayer space for high-performance photovoltaics, *J. Am. Chem. Soc.*, 2019, **141**(6), 2684.

79 J.-C. Blancon, H. Tsai, W. Nie, C. C. Stoumpos, L. Pedesseau, C. Katan, M. Kepenekian, C. M. M. Soe, K. Appavoo and M. Y. Sfeir, Extremely efficient internal exciton dissociation through edge states in layered 2D perovskites, *Science*, 2017, **355**(6331), 1288.

80 J. Zhou, Y. Chu and J. Huang, Photodetectors based on two-dimensional layer-structured hybrid lead iodide perovskite semiconductors, *ACS Appl. Mater. Interfaces*, 2016, **8**(39), 25660.

81 R. Dong, C. Lan, X. Xu, X. Liang, X. Hu, D. Li, Z. Zhou, L. Shu, S. Yip and C. Li, Novel series of quasi-2D Ruddlesden–Popper perovskites based on short-chained spacer cation for enhanced photodetection, *ACS Appl. Mater. Interfaces*, 2018, **10**(22), 19019.

82 D. Yu, F. Cao, Y. Shen, X. Liu, Y. Zhu and H. Zeng, Dimensionality and interface engineering of 2D homologous perovskites for boosted charge-carrier transport and photodetection performances, *J. Phys. Chem. Lett.*, 2017, **8**(12), 2565.

83 Z. Xu, Y. Li, X. Liu, C. Ji, H. Chen, L. Li, S. Han, M. Hong, J. Luo and Z. Sun, Highly sensitive and ultrafast responding array photodetector based on a newly tailored 2D lead iodide perovskite crystal, *Adv. Opt. Mater.*, 2019, 7(11), 1900308.

84 X. Zhang, C. Ji, X. Liu, S. Wang, L. Li, Y. Peng, Y. Yao, M. Hong and J. Luo, Solution-Grown Large-Sized Single-Crystalline 2D/3D Perovskite Heterostructure for Self-Powered Photodetection, *Adv. Opt. Mater.*, 2020, **8**(19), 2000311.

85 Z. Li, Y. Zhao, W. Li, Y. Peng, W. Zhao, Z. Wang, L. Shi and W. Fei, A self-powered flexible UV-visible photodetector with high photosensitivity based on $BiFeO_3/$

XTiO$_3$ (Sr, Zn, Pb) multilayer films, *J. Mater. Chem. A*, 2022, **10**(16), 8772.

86 J. Mao, B. Zhang, Y. Shi, X. Wu, Y. He, D. Wu, J. Jie, C. S. Lee and X. Zhang, Conformal MoS$_2$/silicon nanowire array heterojunction with enhanced light trapping and effective interface passivation for ultraweak infrared light detection, *Adv. Funct. Mater.*, 2022, **32**(11), 2108174.

87 T. Chen, C. Wang, G. Yang, Q. Lou, Q. Lin, S. Zhang and H. Zhou, Monolithic Integration of Perovskite Photoabsorbers with IGZO Thin-Film Transistor Backplane for Phototransistor-Based Image Sensor, *Adv. Mater. Technol.*, 2022, 2200679.

88 E. Talamas Simola, V. Kiyek, A. Ballabio, V. Schlykow, J. Frigerio, C. Zucchetti, A. De Iacovo, L. Colace, Y. Yamamoto and G. Capellini, CMOS-compatible bias-tunable dual-band detector based on GeSn/Ge/Si coupled photodiodes, *ACS Photonics*, 2021, **8**(7), 2166.

89 L. Li, Z. Sun, P. Wang, W. Hu, S. Wang, C. Ji, M. Hong and J. Luo, Tailored engineering of an unusual (C$_4$H$_9$NH$_3$)$_2$(CH$_3$NH$_3$)$_2$Pb$_3$Br$_{10}$ two-dimensional multi-layered perovskite ferroelectric for a high-performance photodetector, *Angew. Chem.*, 2017, **129**(40), 12318.

90 Y. Zhang, Y. Liu, Z. Xu, H. Ye, Q. Li, M. Hu, Z. Yang and S. F. Liu, Two-dimensional (PEA)$_2$ PbBr$_4$ perovskite single crystals for a high performance UV-detector, *J. Mater. Chem. C*, 2019, **7**(6), 1584.

91 C. Ji, D. Dey, Y. Peng, X. Liu, L. Li and J. Luo, Ferroelectricity-Driven Self-Powered Ultraviolet Photodetection with Strong Polarization Sensitivity in a Two-Dimensional Halide Hybrid Perovskite, *Angew. Chem.*, 2020, **132**(43), 19095.

92 Y. Zhang, Y. Liu, Z. Xu, Z. Yang and S. Liu, 2D Perovskite Single Crystals with Suppressed Ion Migration for High-Performance Planar-Type Photodetectors, *Small*, 2020, **16**(42), 2003145.

93 S. Wang, Y. Chen, J. Yao, G. Zhao, L. Li and G. Zou, Wafer-sized 2D perovskite single crystal thin films for UV photo-detectors, *J. Mater. Chem. C*, 2021, **9**(20), 6498.

94 L. Li, J. Li, S. Lan, G. Lin, J. Wang, H. Wang, Y. Xuan, H. Luo and D. Li, Two-step growth of 2D organic–inorganic perovskite microplates and arrays for functional optoelectronics, *J. Phys. Chem. Lett.*, 2018, **9**(16), 4532.

95 X. Fu, S. Jiao, Y. Jiang, L. Li, X. Wang, C. Zhu, C. Ma, H. Zhao, Z. Xu and Y. Liu, Large-scale growth of ultrathin low-dimensional perovskite nanosheets for high-detectivity photodetectors, *ACS Appl. Mater. Interfaces*, 2019, **12**(2), 2884.

96 M. Min, R. F. Hossain, N. Adhikari and A. B. Kaul, Inkjet-printed organohalide 2D layered perovskites for high-speed photodetectors on flexible polyimide substrates, *ACS Appl. Mater. Interfaces*, 2020, **12**(9), 10809.

97 J. Cherusseri, S. J. Varma, B. Pradhan, J. Li, J. Kumar, E. Barrios, M. Z. Amin, A. Towers, A. Gesquiere and J. Thomas, Synthesis of air-stable two-dimensional nano-platelets of Ruddlesden–Popper organic–inorganic hybrid perovskites, *Nanoscale*, 2020, **12**(18), 10072.

98 D. Fu, J. Yuan, S. Wu, Y. Yao, X. Zhang and X.-M. Zhang, A two-dimensional bilayered Dion–Jacobson-type perovskite hybrid with a narrow bandgap for broadband photodetection, *Inorg. Chem. Front.*, 2020, **7**(6), 1394.

99 T. Yang, Y. Li, S. Han, Z. Xu, Y. Liu, X. Zhang, X. Liu, B. Teng, J. Luo and Z. Sun, Highly-Anisotropic Dion–Jacobson Hybrid Perovskite by Tailoring Diamine into CsPbBr$_3$ for Polarization-Sensitive Photodetection, *Small*, 2020, **16**(14), 1907020.

100 Z. Lai, R. Dong, Q. Zhu, Y. Meng, F. Wang, F. Li, X. Bu, X. Kang, H. Zhang and Q. Quan, Bication-Mediated Quasi-2D Halide Perovskites for High-Performance Flexible Photodetectors: From Ruddlesden–Popper Type to Dion–Jacobson Type, *ACS Appl. Mater. Interfaces*, 2020, **12**(35), 39567.

101 C. Fang, M. Xu, J. Ma, J. Wang, L. Jin, M. Xu and D. Li, Large optical anisotropy in two-dimensional perovskite [CH(NH$_2$)$_2$][C(NH$_2$)$_3$]PbI$_4$ with corrugated inorganic layers, *Nano Lett.*, 2020, **20**(4), 2339.

102 M. Prins, K. O. Grosse-Holz, G. Müller, J. Cillessen, J. Giesbers, R. Weening and R. Wolf, A ferroelectric trans-parent thin-film transistor, *Appl. Phys. Lett.*, 1996, **68**(25), 3650.

103 C. R. Kagan, D. B. Mitzi and C. D. Dimitrakopoulos, Organic-inorganic hybrid materials as semiconducting channels in thin-film field-effect transistors, *Science*, 1999, **286**(5441), 945.

104 D. B. Mitzi, C. D. Dimitrakopoulos, J. Rosner, D. R. Medeiros, Z. Xu and C. Noyan, Hybrid field-effect transistor based on a low-temperature melt-processed channel layer, *Adv. Mater.*, 2002, **14**(23), 1772.

105 M. K. Li, T. P. Chen, Y. F. Lin, C. M. Raghavan, W. L. Chen, S. H. Yang, R. Sankar, C. W. Luo, Y. M. Chang and C. W. Chen, Intrinsic Carrier Transport of Phase-Pure Homologous 2D Organolead Halide Hybrid Perovskite Single Crystals, *Small*, 2018, **14**(52), 1803763.

106 H. Zhu, A. Liu, K. I. Shim, J. Hong, J. W. Han and Y. Y. Noh, High-performance and reliable lead-free layered-perovskite transistors, *Adv. Mater.*, 2020, **32**(31), 2002717.

107 Y. Liu, P.-A. Chen, X. Qiu, J. Guo, J. Xia, H. Wei, H. Xie, S. Hou, M. He and X. Wang, Doping of Sn-based two-dimensional perovskite semiconductor for high-perform-ance field-effect transistors and thermoelectric devices, *iScience*, 2022, **25**(4), 104109.

108 Y. Magari, T. Kataoka, W. Yeh and M. Furuta, High-mobi-lity hydrogenated polycrystalline In$_2$O$_3$ (In$_2$O$_3$:H) thin-film transistors, *Nat. Commun.*, 2022, **13**(1), 1.

109 D. B. Mitzi, C. D. Dimitrakopoulos and L. L. Kosbar, Structurally tailored organic–inorganic perovskites: optical properties and solution-processed channel materials for thin-film transistors, *Chem. Mater.*, 2001, **13**(10), 3728.

110 C. Kagan, T. Breen and L. Kosbar, Patterning organic–inorganic thin-film transistors using microcontact printed templates, *Appl. Phys. Lett.*, 2001, **79**(21), 3536.

111 T. Matsushima, K. Fujita and T. Tsutsui, High field-effect hole mobility in organic-inorganic hybrid thin films prepared by vacuum vapor deposition technique, *Jpn. J. Appl. Phys.*, 2004, **43**(9A), L1199.

112 T. Matsushima, F. Mathevet, B. Heinrich, S. Terakawa, T. Fujihara, C. Qin, A. S. Sandanayaka, J.-C. Ribierre and C. Adachi, N-channel field-effect transistors with an organic-inorganic layered perovskite semiconductor, *Appl. Phys. Lett.*, 2016, **109**(25), 253301.

113 C. Chen, X. Zhang, G. Wu, H. Li and H. Chen, Visible-Light Ultrasensitive Solution-Prepared Layered Organic–Inorganic Hybrid Perovskite Field-Effect Transistor, *Adv. Opt. Mater.*, 2017, **5**(2), 1600539.

114 Y. Gao, Z. Wei, P. Yoo, E. Shi, M. Zeller, C. Zhu, P. Liao and L. Dou, Highly stable lead-free perovskite field-effect transistors incorporating linear π-conjugated organic ligands, *J. Am. Chem. Soc.*, 2019, **141**(39), 15577.

115 F. Zhang, H. Zhang, L. Zhu, L. Qin, Y. Wang, Y. Hu, Z. Lou, Y. Hou and F. Teng, Two-dimensional organic–inorganic hybrid perovskite field-effect transistors with polymers as bottom-gate dielectrics, *J. Mater. Chem. C*, 2019, **7**(14), 4004.

116 F. Liu, L. Wang, J. Wang, F. Wang, Y. Chen, S. Zhang, H. Sun, J. Liu, G. Wang and Y. Hu, 2D Ruddlesden–Popper perovskite single crystal field-effect transistors, *Adv. Funct. Mater.*, 2021, **31**(1), 2005662.

117 Y. Reo, H. Zhu, J.-Y. Go, K. In Shim, A. Liu, T. Zou, H. Jung, H. Kim, J. Hong and J. W. Han, Effect of Monovalent Metal Iodide Additives on the Optoelectric Properties of Two-Dimensional Sn-Based Perovskite Films, *Chem. Mater.*, 2021, **33**(7), 2498.

118 S. Wang, S. Frisch, H. Zhang, O. Yildiz, M. Mandal, N. Ugur, B. Jeong, C. Ramanan, D. Andrienko and H. I. Wang, Grain engineering for improved charge carrier transport in two-dimensional lead-free perovskite field-effect transistors, *Mater. Horiz.*, 2022, **9**(10), 2633.

119 J.-Y. Go, H. Zhu, Y. Reo, H. Kim, A. Liu and Y.-Y. Noh, Sodium Incorporation for Enhanced Performance of Two-Dimensional Sn-Based Perovskite Transistors, *ACS Appl. Mater. Interfaces*, 2022, **14**(7), 9363.

120 Y. Gao, Z. Wei, S.-N. Hsu, B. W. Boudouris and L. Dou, Two-dimensional halide perovskites featuring semiconducting organic building blocks, *Mater. Chem. Front.*, 2020, **4**(12), 3400.

121 J. V. Milić, Multifunctional layered hybrid perovskites, *J. Mater. Chem. C*, 2021, **9**(35), 11428.